

1 **Stably Stratified Canopy Flow in Complex Terrain**

2

3 Xiyan Xu^{1,2}, Chuixiang Yi^{1,2,3*}, Eric Kutter^{1,2}

4 ¹*Queens College, City University of New York, Flushing, NY 11367, USA*

5 ²*The Graduate Center, City University of New York, New York, NY 10016, USA*

6 ³*Department of Meteorology, Bert Bolin Centre for Climate Research, Stockholm University,*
7 *Stockholm S-106 91, Sweden*

8 *Correspondence: Chuixiang Yi

9

10 School of Earth and Environmental Sciences

11 Queens College, City University of New York

12 65-30 Kissena Blvd

13 Flushing, New York 11367

14 Phone: (718) 997-3366

15 Fax: (718) 997-3299

16 E-mail: cyi@qc.cuny.edu

1 **Abstract**

2 Stably stratified canopy flow in complex terrain has been considered a difficult condition
3 for measuring net ecosystem–atmosphere exchanges of carbon, water vapor, and energy.

4 A long-standing advection error in eddy-flux measurements is caused by stably-stratified
5 canopy flow. Such a condition with strong thermal gradient and less turbulent air is also
6 difficult for modeling. To understand the challenging atmospheric condition for eddy-

7 flux measurements, we use the Renormalized Group (RNG) k - ϵ turbulence model to
8 investigate the main characteristics of stably stratified canopy flows in complex terrain.

9 In this two-dimensional simulation, we imposed persistent constant heat flux at ground
10 surface and linearly increasing cooling rate in the upper canopy layer, vertically varying

11 dissipative force from canopy drag elements, buoyancy forcing induced from thermal
12 stratification and the hill terrain. These strong boundary effects keep nonlinearity in the
13 two-dimensional Navier-Stokes equations high enough to generate turbulent behavior.

14 The fundamental characteristics of nighttime canopy flow over complex terrain measured
15 by the small number of available multi-tower advection experiments can be reproduced

16 by this numerical simulation, such as: (1) unstable layer in the canopy and super-stable
17 layers associated with flow decoupling in deep canopy and near the top of canopy, (2)

18 subcanopy drainage flow and drainage flow near the top of canopy in calm night, (3)
19 upward momentum transfer in canopy, downward heat transfer in upper canopy and

20 upward heat transfer in deep canopy and (4) large buoyancy suppression and weak shear
21 production in strong stability.

22 **Keywords:** Canopy flow, complex terrain, stable stratification, Richardson number,

23 turbulent kinetic energy, CFD, RNG k - ϵ model

1 **1 Introduction**

2 Canopy flow occurring within and immediately above vegetation canopies plays a
3 substantial role in regulating atmosphere-biosphere interaction. The canopy layer is an
4 interface between land and atmosphere, in which most natural resources humans need are
5 produced by biochemical reactions. Canopy flow influences those biochemical processes
6 through the control of gas exchange between the vegetation and the atmosphere (e.g.,
7 influencing reaction rates by changing gas concentrations), heat exchanges (e.g.,
8 influencing reaction conditions by changing temperature), and momentum exchanges
9 (e.g., changing turbulent mixing conditions). Better understanding of canopy flow
10 behavior has many practical implications in accurately determining, for instance,
11 terrestrial carbon sinks and sources (Sun et al., 2007), the fate of ozone within and above
12 forested environments (Wolf et al., 2011), forest fire spread rate (Cruz et al., 2005), bark
13 beetle management (Edburg et al., 2010), and others.

14 The typical patterns of forest canopy turbulent flows are characterized by an S-
15 shaped wind profile with an exponential Reynolds stress profile rather than the widely-
16 used logarithmic wind profile and constant Reynolds stress observed over bare ground
17 (Yi, 2008). S-shaped wind profiles have been observed within forest canopies in
18 numerous studies (Baldocchi and Meyers, 1988; Bergen, 1971; Fons, 1940; Lalic and
19 Mihailovic, 2002; Landsberg and James, 1971; Lemon et al., 1970; Meyers and Paw U,
20 1986; Oliver, 1971; Shaw, 1977; Turnipseed et al., 2003; Yi et al., 2005; Queck and
21 Bernhofer, 2010; Sypka and Starzak, 2013). The S-shaped profile refers to a secondary
22 wind maximum that is often observed within the trunk space of forests and a secondary
23 minimum wind speed in the region of greatest foliage density. The features of S-shaped

1 wind profiles imply that K-theory and mixing-length theory break down within a forest
2 canopy layer (Denmead and Bradley, 1985; Yi, 2008). Particularly, the assumption of a
3 constant mixing-length within a canopy is not consistent with the original mixing-length
4 theory. This is because a mixing-length (l_m) must satisfy von Karman's rule (von
5 Karman, 1930; Schlichting, 1960; Tennekes and Lumley, 1972), which indicates that a
6 mixing length is a function of velocity distribution (Schlichting, 1960), as:

$$l_m = \kappa \left| \frac{dU/dz}{d^2U/dz^2} \right|$$

7 where κ is von Karman's constant, U is wind speed, and z is height within the canopy..
8 The mixing length of the S-shaped velocity distribution is not constant, being minimum
9 at the local extreme values of the wind profile ($dU/dz = 0$, $d^2U/dz^2 \neq 0$) and
10 maximum at the inflection point of the wind profile ($dU/dz \neq 0$, $d^2U/dz^2 = 0$) (Wang
11 and Yi, 2012). A mixing-length that varies with height within canopy has been
12 demonstrated by large-eddy simulations (Coceal et al., 2006; Ross, 2008) and by water
13 tank experiments (Poggi and Katul, 2007a).

14 The features of S-shaped wind profiles also dictate the existence of super-stable
15 layers near levels where wind speed is maximum (or minimum) and temperature
16 inversion (temperature increasing with height) exists, leading the Richardson number to
17 be extremely large or infinity (Yi et al., 2005). A super-stable layer acts as a 'lid' or
18 'barrier' that separates fluid into two uncorrelated layers: (1) the lower layer between the
19 ground and the super-stable layer, and (2) the upper layer above the super-stable layer.
20 This canopy flow separation was verified by SF₆ diffusion observations (Yi et al., 2005)
21 and carbon isotope experiments (Schaeffer et al., 2008). The lower layer is sometimes
22 called a 'decoupled layer' (Alekseychik et al., 2013) that is shallow, usually within the

1 trunk space of a forest. Because the super-stable layer prohibits vertical exchanges, the
2 decoupled layer channels air in the horizontal direction. The characteristics of the
3 channeled air are highly dependent on soil conditions, containing a high concentration of
4 soil respired CO₂ and soil evaporated water vapor, and consisting of colder air cooled by
5 radiative cooling at the ground surface (Schaeffer et al., 2008). The channeled air is
6 sometimes termed ‘drainage flow’, and is a common phenomenon in hilly terrains under
7 stable atmospheric conditions, such as on calm and clear nights (Yi et al., 2005;
8 Alekseychik et al., 2013). The drainage flow limits the accuracy of tower-based estimates
9 of ecosystem-atmosphere exchanges of carbon, water, and energy. Sensors on the tower
10 above the canopy cannot measure the fluxes conducted by drainage flow because the
11 layer above the canopy is decoupled from the drainage flow by the isolating super-stable
12 layer. This advection problem is a well-known issue that has not yet been solved using
13 eddy-flux measurements (Goulden et al., 1996; Aubinet et al., 2003; Staebler and
14 Fitzjarrald, 2004; Sun et al., 2007; Yi et al., 2008; Montagnani et al., 2009; Feigenwinter
15 et al., 2010; Aubinet and Feigenwinter, 2010; Queck and Bernhofer, 2010; Tóta et al.,
16 2012; Siebicke et al., 2012).

17 The concept of a super-stable layer is useful in interpreting data associated with
18 stratified canopy air (Schaeffer et al., 2008). However, stratified canopy flows over
19 complex terrain are far too complex to be able to characterize considering only a super-
20 stable layer. Canopy structure (quantified by leaf area density profile), terrain slope, and
21 thermal stratification are three key parameters in understanding the details of stratified
22 canopy flows over complex terrain. The thermal stratification plays a leading role in the
23 development of pure sub-canopy drainage flows (Chen and Yi, 2012): strong thermal

1 stratification favors drainage flow development on gentle slopes, while weak or near-
2 neutral stratification favors drainage flow development on steep slopes. We speculate that
3 interaction between thermal stratification and terrain slopes and vegetation canopy may
4 result in multiple super-stable layers. The complicated thermal and flow patterns cause
5 difficulties in understanding the mechanisms and rates of exchange of mass and energy
6 between the terrestrial biosphere and the atmosphere (Alekseychik et al., 2013; Burn et
7 al., 2011; Yi et al., 2005).

8 In this paper, we attempt to use a computational fluid dynamics (CFD) technique
9 to examine the micro-structure of stratified canopy flows to provide insight into the role
10 of physical processes that govern drainage motion and its turbulent characteristics within
11 canopy in complex terrain. There are many challenges to face when pursuing this goal.
12 First, the mixing-length theory and K-theory that are widely used as closure approaches
13 to momentum equations (Wilson et al., 1998; Pinard and Wilson, 2001; Ross and Vosper,
14 2005; Katul et al., 2006) have been shown to have questionable validity within a forest
15 canopy layer both theoretically (Yi, 2008) and observationally (Denmead and Bradley,
16 1985). Second, the analytical model (Finnigan and Belcher, 2004) is limited to neutral
17 condition and hills of gentle slope. The analytical model is developed based on the
18 linearized perturbation theory for the flow over a rough hill (Jackson and Hunt, 1975),
19 which assumes that the mean flow perturbations caused by the hill are small in
20 comparison to the upwind flow. Poggi and Katul (2007b) and Ross and Vosper (2005)
21 have shown that the analytical model fails to model the flow pattern on dense canopies on
22 narrow hills. Third, even though turbulence closure models and large eddy simulation
23 models have been used to simulate flow within and above the canopy in numerous

1 published studies, most numerically reproduced canopy flow is confined to idealized
2 cases: either neutral (Ross and Vosper, 2005; Dupont et al., 2008; Ross, 2008) or weakly
3 unstable (Wang, 2010) atmospheric conditions; or flat terrain with a homogeneous and
4 extensive canopy (Huang et al., 2009; Dupont et al., 2010).

5 Simulations of stratified canopy flow have received little consideration. This
6 might be attributed to difficulties in numerical simulations arising from small scales of
7 motion due to stratification (Basu et al., 2006), and complex interaction between wind
8 and canopy drag elements (Graham and Meneveau, 2012). Large eddy simulation has
9 been quite successful in producing turbulent flow and its related scalar transport in
10 neutral and unstable cases (Shen and Leclerc, 1997; Wang, 2010; Mao et al., 2008).
11 However, under stable conditions, due to flow stratification, the characteristic size of
12 eddies becomes increasingly small with increasing atmospheric stability, which
13 eventually imposes an additional burden on the LES-SGS models (Basu et al., 2010). If
14 resolution is high enough, any turbulent flow can be simulated accurately by LES. In fact,
15 given sufficiently fine resolution, LES becomes Direct Numerical Simulation (DNS),
16 demanding very fine spatial and temporal resolution (Galperin and Orszag, 1993), which
17 is currently beyond the reach of available computational power.

18 In this paper, we employ the renormalized group (RNG) k - ε turbulence model to
19 investigate stably stratified canopy flows in complex terrain. The RNG k - ε turbulence
20 model was developed by Yakhot and Orszag (1986a) using the renormalized group
21 methods and prescribes the turbulent length scale related to transport of turbulent kinetic
22 energy and dissipation rate (Yakhot and Orszag, 1986b; Smith and Reynolds, 1992).
23 Compared to standard k - ε turbulence model, the numerically derived parameters are not

1 subject to experimental adjustment in RNG $k-\varepsilon$ turbulence model. The rate of strain term
2 in the dissipate transport equation is important for treatment of flows in rapid distortion
3 limit, e.g. separated flows and stagnated flows (Biswas, and Eswaran, 2002) which
4 commonly occur in vegetated hilly terrain. The initial successes in applying the RNG $k-\varepsilon$
5 turbulence model to generate airflows in hilly terrain have been demonstrated by Kim
6 and Patel (2000) and Xu and Yi (2013).

7 **2 Method**

8 **2.1. Numerical implementation**

9 The two dimensional computational domain extends over 1400m×130m in a
10 Cartesian coordinate system, corresponding to 1200×157 grid intervals in the x and y
11 directions. A single hill is 100m long covered with a 15m tall homogeneous forest
12 canopy, which extends from 650m of the domain in horizontal. The mesh spacing in both
13 horizontal and vertical at the forested hill is 0.5m and is stretched with a power law,
14 starting with a grid spacing of 0.5m throughout the canopy, with a larger grid spacing
15 stretching outwards from the edge of the forest and the top of the canopy on the hill crest.
16 The stretch power in both horizontal and vertical is 1.15. Ground surface roughness
17 height is set to be 0.01m.

18 In this study, the topography is specified with a ridge-like sinusoidal hill, infinite
19 in the unsimulated third dimension. The shape function of the hill in 2D is defined as

$$H(x) = \frac{H}{2} \cos\left(\frac{\pi x}{2L}\right) + \frac{H}{2} \quad (1)$$

20

1 where H is the hill height, L is the half length scale (half of the hill width at mid-slope
 2 height), x is longitudinal distance with $x = 0$ at the center of the single hill. The variation
 3 of the slope (H/L) is specified by changing H with a constant $L = 25$ m.

4 The porous canopy layer (canopy height $h = 15$ m) is designed horizontally
 5 homogeneous along the slope. Leaf area density profile $a(z)$ is specified as values from
 6 observation of an actual forest (Yi et al., 2005) with the maximum leaf area density at
 7 about 8m. Leaf area index (LAI) is 3.3. The ambient temperature is $\theta_0(z) = \theta_{00} + \gamma z$,
 8 where $\theta_{00} = 288K$, is the potential temperature at $z = 0$, γ is ambient lapse rate, set to -
 9 6°C km^{-1} . The cooling rate at ground surface is set to -15 Wm^{-2} . Since we are most
 10 interested in calm night-time conditions, no wind in the domain is initially specified. The
 11 fixed pressure boundary condition (open boundary) is applied to lateral boundaries and
 12 top-boundary, where the pressure is close to 0.0 Pa, relative to the external pressure.

13 2.2. Conservation of mass and momentum

14 The flow is assumed to be steady and the Boussinesq approximation is applied.
 15 The mass, momentum, and energy balance equations in the canopy sub-layer can be
 16 written as:

$$\frac{\partial \bar{u}_j}{\partial x_i} = 0 \quad (2)$$

17

$$\bar{u}_j \frac{\partial \bar{u}_i}{\partial x_j} = -\frac{1}{\rho} \frac{\partial P_*}{\partial x_i} + \nu \frac{\partial^2 \bar{u}_i}{\partial x_i \partial x_j} - \frac{\partial}{\partial x_j} (\overline{u'_i u'_j}) - g_i \beta (\bar{\theta} - \theta_\infty) - F_{Di} \quad (3)$$

18

$$\bar{u}_j \frac{\partial \bar{\theta}}{\partial x_j} = \Gamma \frac{\partial^2 \bar{\theta}}{\partial x_i \partial x_j} - \frac{\partial}{\partial x_j} (\overline{\theta' u'_j}) + \frac{1}{\rho c_p} Q_{source} \quad (4)$$

1 where \bar{u}_i and \bar{u}_j are the mean velocity components along x_i and x_j direction,
2 respectively, $\bar{\theta}$ is the mean potential temperature, u'_i , u'_j and θ' are the
3 fluctuations from their mean value \bar{u}_i , \bar{u}_j and $\bar{\theta}$, ρ is the air density, ν is kinematic
4 viscosity of air, P_* is the deviation of pressure from its reference value, β is the
5 thermal expansion coefficient of air, and θ_∞ is the reference temperature, g_i is the
6 gravity acceleration in i direction, $\Gamma = \nu/P_r$ is thermal diffusion coefficient,
7 turbulent Prandtl number P_r is 0.5 in canopy layer and 1 above the canopy. $P_r =$
8 0.5 is close to the values used in large-eddy simulations of stably stratified
9 atmospheric boundary layer turbulence (Basu and Porté-Agel, 2006; Stoll and
10 Porté-Agel, 2008). In most of the region above the canopy (except very near the
11 top of canopy), turbulence is very weak. In this region, molecular effects are
12 dominant, especially in conditions without synoptic wind. Q_{source} is the energy
13 source. When the atmosphere is stably stratified, $Q_{source} < 0$ indicating radiative
14 cooling of the canopy elements and ground surface. The constant cooling rate at
15 the surface can drive a steady state stable boundary layer on flat and sloped
16 terrain (Brost and Wyngaard, 1978), so we set $Q_{source} = 0$ in the lower canopy
17 layer (0-8m) and then linearly decreased to -8 Wm^{-3} at the top canopy layer. The
18 thermal conditions are sufficient to drive fully developed turbulent flows,
19 according to dimensional analysis of the bulk Reynolds number :

$$Re_b = \frac{h_i U}{\nu} = \frac{O(10^1 m) \times O(10^{-1} m s^{-1})}{O(10^{-5} m^2 s^{-1})} = O(10^5)$$

20 where h_i is the depth of boundary layer, U is bulk velocity and ν is kinematic
21 viscosity.

22

1 The steady state assumption is satisfied with condition proposed by Mahrt (1982),

$$F\hat{H}/\hat{T} \ll 1 \quad (5)$$

2 where F is the Froude number, \hat{H} is the ratio of the average flow depth H to the surface
3 elevation drop ΔZ_s , and \hat{T} is the ratio of the time scale T to the Lagrangian time L/U . The
4 Froude number is defined as

$$F = U^2 / \left(g \frac{\Delta\theta}{\theta_0} H \right) \quad (6)$$

5 where U is downslope velocity scale ($= O(10^{-1}) \text{ m s}^{-1}$), g is gravity acceleration ($= 9.81 \text{ m}$
6 s^{-2}), $\Delta\theta$ is scale value for potential temperature deficit of the canopy layer ($= O(10^0) \text{ K}$),
7 θ_0 is the basic state potential temperature ($= O(10^2) \text{ K}$), H is the flow depth scale, chosen
8 to be the depth of significant temperature deficit which coincides with the layer of
9 enhanced thermal stratification ($= O(10^1) \text{ m}$). In this simulation setting, $F = O(10^{-2})$.
10 $\hat{H} = H/\Delta Z_s$, where $\Delta Z_s = L \sin\alpha$, L is downslope length scale ($= O(10^1) \text{ m}$),
11 $\sin\alpha(\%) = O(10^1)$. Thus, $\hat{H} = O(10^0)$. $\hat{T} = TU/L$, where $T = O(10^4) \text{ s}$ is suggested by
12 Mahrt (1982) to represent the order of magnitude of temporal accelerations
13 associated with the diurnal evolution of drainage circulations. In our simulation,
14 $\hat{T} = O(10^2)$. Thus, $F\hat{H}/\hat{T} = O(10^{-4}) \ll 1$.

15 F_{Di} is the drag force exerted by the canopy elements in i direction,

$$F_{Di} = \frac{1}{2} K_r u_i |U| \quad (7)$$

16 where K_r is the resistance coefficient, which is derived from an empirical relationship
17 given by Hoener (1965),

$$K_r = \frac{1}{2} \left[\frac{3}{2\phi} - 1 \right]^2 \quad (8)$$

1 where ϕ is porosity of the canopy layer, which can be obtained from leaf area density
 2 profile $a(z)$ (Gross, 1993),

$$\phi(z) = \frac{\sqrt{1 + 4a(z)} + 1}{2a(z)} \quad (9)$$

3 F_{Di} is zero above the canopy.

4 **2.3. RNG k - ε model**

5 The RNG model was developed by Yakhot and Orszag (1986a; b; Yakhot et al.,
 6 1992) using Re-Normalization Group (RNG) methods. The RNG k - ε turbulent model has
 7 been successfully applied in reproducing topographic and canopy related flows (Kim and
 8 Patel, 2000; Xu and Yi, 2013; Pattanapol et al., 2007).

9 In RNG k - ε model, the Reynolds stress in Eq. (3) and turbulent heat flux in Eq.
 10 (4), respectively, are solved by turbulent viscosity, as:

$$-\overline{u'_i u'_j} = \mu_t \left(\frac{\partial \bar{u}_i}{\partial x_j} + \frac{\partial \bar{u}_j}{\partial x_i} \right) - \frac{2}{3} \delta_{ij} k \quad (10)$$

$$-\overline{\theta' u'_j} = \mu_\theta \frac{\partial \bar{\theta}}{\partial x_j} \quad (11)$$

11 Where μ_t and $\mu_\theta = \mu_t / Pr$ are the turbulent viscosities of momentum and heat, respectively,
 12 δ_{ij} is Kronecker delta, and k is the turbulent kinetic energy.

13 RNG k - ε model assumes that turbulence viscosity in Eq. (10) is related to
 14 turbulence kinetic energy k (TKE) and dissipation ε :

$$\mu_t = \rho C_\mu \frac{k^2}{\varepsilon} \quad (12)$$

- 1 where k and ε are determined from the transport equations for k and ε ; C_μ is a
 2 dimensionless constant.

- 3 The steady state transport equations for k and its dissipation ε are written as:

$$\bar{u}_i \frac{\partial k}{\partial x_i} = \frac{\partial}{\partial x_i} \left(\frac{\mu_t}{\sigma_k} \frac{\partial k}{\partial x_i} \right) + P_s + P_b + P_w + T_p - \varepsilon \quad (13)$$

$$\bar{u}_i \frac{\partial \varepsilon}{\partial x_i} = \frac{\partial}{\partial x_i} \left(\frac{\mu_t}{\sigma_\varepsilon} \frac{\partial \varepsilon}{\partial x_i} \right) + C_{\varepsilon 1} \frac{\varepsilon}{k} P_s - \rho C_{\varepsilon 2} \frac{\varepsilon^2}{k} - S \quad (14)$$

- 4 where P_s is shear production, given by:

$$P_s = \mu_t \frac{\partial \bar{u}_i}{\partial x_j} \left(\frac{\partial \bar{u}_i}{\partial x_j} + \frac{\partial \bar{u}_j}{\partial x_i} \right) \quad (15)$$

- 5 P_b is buoyancy production, given by:

$$P_b = -\mu_\theta g_i \beta \frac{\partial \bar{\theta}}{\partial x_i} \quad (16)$$

- 6 P_w is wake production caused by canopy elements as (Meyers and Baldocchi, 1991):

$$P_w = \bar{u}_i F_{Di} = \frac{1}{2} K_r |U| \bar{u}_i^2 \quad (17)$$

- 7 T_p is pressure collection term, which is calculated as residual of other TKE
 8 components, S is a volumetric source term which includes the rate-of-strain, given
 9 by:

$$S = \frac{C_\eta \eta^3 \left(1 - \frac{\eta}{\eta_0} \right) \varepsilon^2}{(1 + \beta_0 \eta^3) k} \quad (18)$$

$$\eta = \frac{k}{\varepsilon} \left[\frac{P_s}{\mu_t} \right]^{1/2} \quad (19)$$

1 where the empirical constants C_μ , σ_k , σ_ε , $C_{\varepsilon 1}$, $C_{\varepsilon 2}$, β_0 , and η_0 are 0.0845, 0.7194, 0.7194,
2 1.42, 1.68, 0.012, and 4.38, respectively (Yakhot and Orszag, 1986a; b).

3 **3 Results and discussion**

4 After a quasi-equilibrium condition is approached, all the solved fields in the
5 studied cases are developed to be near symmetric horizontally (in the x -direction) with
6 respect to the center of the modeled hill at $x = 0$ due to the homogeneous boundary
7 conditions and initial settings. We restrict our discussion to the right half of the hill. Our
8 results show (Fig. 1) that wind structure is differentiated into down-sweep ($H/L \leq 0.6$)
9 and up-draft ($H/L \geq 0.8$) within canopy. The temperature, wind and turbulence
10 characteristics on representative gentle ($H/L = 0.6$) and steep ($H/L = 1.0$) hills are
11 illustrated (see Fig. 1) to explore the thermal and mechanical processes that govern the
12 airflow structures.

13 **3.1 Thermal analysis**

14 In the model, strong stratification develops with distinct thermal distribution on the
15 slope, subject to heat loss on the slope surface and the upper canopy layer. The
16 heterogeneous distribution of heat within the canopy causes a ‘fish-head’-shaped
17 temperature distribution on the slope, with the upper jaw in the upper canopy layer and
18 the lower jaw attaching to the slope surface. The jaws consist of cold air while the open
19 mouth shows relatively warmer air (Fig. 2). In comparison with the upper jaw which is
20 confined to the middle and lower slope, the lower jaw extends up to the crest of the hill.

1 As the slope intensity is reduced, the fish-head effect's upper jaw is diminished. For a
2 very gentle slope (i.e., $H/L \ll 1$), the model produces a horizontal isotherm pattern with
3 cold air at the bottom of the slope and warm air upslope, as would be expected in real-
4 world conditions. A significant difference in temperature distribution among varied
5 slopes results in a different angle of orientation of the fish-head temperature profile.
6 Isotherms are inclined parallel to the slope surface because they tend to follow the shape
7 of the slope and the top-canopy layer since the cooling along the slope surface is uniform.
8 The temperature distribution on a gentle hill is shown as an angled fish-head shape, while
9 the fish-head is tilted by the slope on the steep hill, which is shown by the isotherms on
10 the lower jaws. The different fish-head profile's angle can explain specific flow
11 structures in the canopy (see sect. 3.2). In accordance with the fish-head temperature
12 distribution, temperature profiles are shown in three layers (Fig. 3a-d). A strong inversion
13 layer is developed across the lower jaw, above which temperature slightly decreases with
14 height in a thermal transition zone and a weak inversion layer is formed across the upper
15 jaw. The temperature gradient and the depth of the lower inversion layer increases, since
16 cold air flowing down the slope results in a cool pool on the lower slope where a single
17 inversion layer extends above the canopy (Fig. 3e, f). The temperature difference from
18 the hill surface to the top of the canopy at the hill crest is about 0.8°C and 0.4°C for
19 gentle and steep hills, respectively, while the difference increases to around 3.2°C in the
20 canopy layer at the feet of both hills. The inversion strength near the surface is larger than
21 in the upper canopy, which is due to the stronger radiative cooling effect on the surface.
22 The temperature gradient and inversion on the steep hill are predicted weaker than on the
23 gentle hill, because at the same horizontal x/L location, the canopy layer is at a higher

1 elevation on the steep hill. Regardless of the horizontal location x/L , we find that
 2 inversions both near the surface and in the upper canopy are stronger on the steep hill
 3 than on the gentle hill at the same elevation, which benefits the development of stronger
 4 drainage flow on the steep slope.

5 The Richardson number (Ri) is the ratio of the relative importance of buoyant
 6 suppression to shear production of turbulence, which is used to indicate dynamic stability
 7 and formation of turbulence. Ri is calculated based on mean profiles of wind and
 8 temperature. For different purposes and data availability, gradient Richardson number
 9 (Ri_g) and bulk Richardson number (Ri_b) are used to predict the stability within canopy. Yi
 10 et al. (2005) found that the gradient Richardson number,

$$Ri_g = \frac{(g/\bar{\theta})(\partial\bar{\theta}/\partial z)}{(\partial\bar{U}/\partial z)^2} \quad (20)$$

11 with $\partial\bar{U}/\partial z = 0$ and $\partial\bar{\theta}/\partial z \neq 0$ at the inflection points of the S-shaped wind profile
 12 resulted in an infinite Ri_g , which describes the super-stable layer. In a forest, wind and
 13 temperature are typically only measured in a few levels, making $\partial\bar{U}/\partial z$ and $\partial\bar{\theta}/\partial z$
 14 impossible to directly calculate. Therefore, Ri_b is commonly used to quantify stability
 15 between two levels (z_1 and z_2) using the measured temperature and wind speed (Zhang et
 16 al., 2010; Burns et al., 2011; Alekseychik et al., 2013),

$$Ri_b = \frac{g}{\bar{\theta}} \frac{\theta(z_2) - \theta(z_1)}{[U(z_2) - U(z_1)]^2} (z_2 - z_1) \quad (21)$$

17 In our modeling setting, the gridding space in vertical is $\Delta z = z_2 - z_1$, which is 0.5m in the
 18 canopy layer. We define a local Richardson number to evaluate stability around the

1 forested hill and examine the local stability in response to the heterogeneous distribution
2 of heat. The local Richardson number in grid (m, n) is calculated as,

$$Ri_l = \frac{g}{\theta_{m,n}} \frac{(\theta_{m,n} - \theta_{m,n-1})(z_{m,n} - z_{m,n-1})}{(u_{m,n} - u_{m,n-1})^2 + (w_{m,n} - w_{m,n-1})^2} \quad (22)$$

3 Local Richardson number indicates that, within the canopy, flow is stably
4 stratified except for an unstable region penetrating from the hill summit into the middle
5 slope within the thermal transition regime (Fig. 1). Ri_l is found to be extremely large (\sim
6 10^5) just above the canopy on the upper to middle slope (Fig. 4, locations a-d) indicating
7 a thin primary super stable layer just above the top of canopy. The primary super stable
8 layer is elevated and deepened on the lower slope (Fig. 4 locations e and f), extended
9 from the height of $1.3-1.4h$ to about the height of $2h$. The deep primary super stable layer
10 is caused by the strong cooling and temperature inversion at the base of the hill,
11 regardless of slope intensity. Within canopy, a secondary super stable layer with
12 extremely high Ri_l is developed below $0.5h$. On the lower slope, the depth of the
13 secondary super stable layer extends from the slope surface up to $0.5h$. The deep
14 secondary super stable layer is consistent with deep and strong temperature inversion
15 layer where wind is stagnated. The absence of a secondary super stable layer on the
16 summit could be explained by stronger mixing of warmer air from above-canopy,
17 because stronger drainage flow promotes the penetration of warm air from aloft when
18 cold air moves down the slope (Zängl, 2003). Air in the transition region with negative
19 temperature gradient is unstably stratified. The transition region is developed by the
20 downwelling of cool air from the upper canopy with relatively warmer air upwelling
21 from the lower canopy. The results show that for a sufficiently steep slope, the effects of

1 the hill dominate the atmospheric profile, while for more gentle slopes the effects of the
2 canopy dominate the resultant atmospheric profile.

3 The nocturnal stable canopy layer could be used to explain the occurrence of
4 within- and above- canopy flows decoupling observed in prior studies. van Gorsel et al.
5 (2011) reported a very stable nighttime canopy layer ($Ri_b > 1$) using the bulk Richardson
6 number, indicating that the canopy layer is decoupled from air aloft. Decoupling at the
7 top of the canopy is more likely to occur as the buoyancy is more dominant and air at the
8 top of the canopy is strongly stable. The canopy top decoupling weakens vertical
9 exchange of mass and heat between the vegetation and the atmosphere aloft. The
10 measurement data show large temperature and CO₂ gradients (Burns et al., 2011) as
11 decoupling occur in strongly stabilized atmosphere. Decoupling at the top of the canopy
12 produced stronger carbon dioxide and temperature gradients than within canopy
13 decoupling (Alekseychik et al., 2013). The primary super stable layer in our study is
14 shown as a lid located at the top and above canopy, which could terminate the vertical
15 exchange between the canopy and the air above. During nighttime, soil respiration
16 contributes about 60-70% (Janssens et al., 2001) of the total CO₂ emission from the
17 terrestrial ecosystem. The soil respired CO₂ could be blocked by the secondary super
18 stable layer forming a very shallow pool on the slope surface.

19 **3.2 Wind flow structures**

20 Figure 1 shows that air above the canopy sinks and converges towards the hill and
21 then shifts direction within canopy. Flow converges to the hill from all sides, and is then
22 inflected near the top of the canopy, following the shape of the slope as drainage flow
23 within the canopy. The height of inflection points increases as the air flows down the

1 slope. The inflection points are approximately at the bottom of the primary super stable
2 layer. As a result of the abrupt convergence in the top of the canopy at the base of the
3 hill, wake vortices are developed near the forest edge, after the wind leaves the hillside
4 within the primary super stable layer. The wake vortices can extend to about $2.6L$ in
5 horizontal and $1.3h$ in vertical. According to the flow location within the canopy, we
6 identify the drainage flow as two streams: the majority air mass within the upper-canopy
7 inversion layer is called the upper-canopy drainage flow (UDF) layer; and the majority
8 air mass within the inversion layer in the lower-canopy is called the lower-canopy
9 drainage flow (LDF) layer. The UDF is developed as the air above the canopy sinks from
10 lateral sides towards slopes of the hill. However, instead of further descending into the
11 canopy, the sinking motion is diverted to follow the shape of the top-canopy layer as it
12 reaches the top of the canopy (Fig. 1 and 6). The UDF accelerates down the slope
13 between the top of the unstable layer and the bottom of the primary super stable layer,
14 reaching its maximum wind speed of 0.3 m s^{-1} at location (Fig. 5d
15 and 6a) on the gentle slope and 0.35 m s^{-1} at location (Fig. 5e and 6b) on the steep slope,
16 and then decelerates down to the feet of the hills. The air sinking over the crest can
17 directly reach the surface of the crest and flow along the slope to form the LDF. The
18 maximum wind speed of the LDF is at location (Fig. 5d) for a gentle slope (0.18 m s^{-1})
19 and at location (Fig. 5c) for a steep slope (0.29 m s^{-1}). The maximum wind speed in LDF
20 occurs on the slope surface, below the secondary super stable layer. Deceleration of the
21 flow towards the base of the hill should occur for a number of reasons. The pool of cool,
22 dense air at the base of the hill resists incoming flow. Also, the drag force acting against
23 the wind is dependent on the speed of the air flow squared.

1 UDF and LDF show different patterns within canopy for different slopes, which
2 essentially regulates the direction of wind shifting within canopy (Fig. 1 and 6). On the
3 gentle slope ($H/L = 0.6$), UDF is much thicker compared with LDF (Fig. 6a). Air in UDF
4 accelerates within the regime of the upper inversion layer reaching its maximum at the
5 top of thermal transition region and then decelerates to a minimum ($u = 0$ and $w = 0$, Fig.
6 5) at the top of the slope surface inversion layer. Then, UDF sweeps horizontally to join
7 the shallow LDF on the slope surface, which is shown as negative streamwise velocity
8 and near-zero vertical velocity in Fig. 5 (down-sweep). When the slope is steep ($H/L =$
9 1.0), UDF is much shallower than LDF on the upper slope. Air in LDF accelerates on the
10 upper slope (Fig. 5a-c), followed by deceleration and stagnation. The stagnated flow
11 jumps perpendicularly from the deep canopy layer to join the shallow UDF in the upper
12 canopy layer (The up-draft, with $u > 0$ and $w > 0$, is visible in Fig. 1 and 5). The shifting
13 winds on both gentle and steep slopes are parallel to the isotherms in the warm ‘fish
14 mouth’ region of the profile. Rotational vortices are formed below the shifting winds.

15 The generation and direction of the shifting-wind structure are primarily driven by
16 the slope and stratification. Under calm and stably stratified conditions, the dominant
17 driving force of sinking drainage flow on the slope is the hydrostatic buoyancy force
18 which is given as: $F_{hs} = g(\Delta\theta/\theta_0) \sin \alpha$, where α is the slope angle, $\Delta\theta$ is the potential
19 temperature difference between the ambient air and the colder slope flow, θ_0 is the
20 ambient potential temperature. The drainage flow on both the gentle and steep slopes is
21 initiated by the dominant F_{hs} as the air is calm and stably stratified (Froude number $\ll 1$,
22 Belcher et al., 2008). The magnitude of F_{hs} increases with slope angle α so that F_{hs} is
23 much larger on a steep slope than a gentle slope, leading to a stronger sinking motion

1 above the crest. The sinking air penetrates to the lower part of the canopy at the hilltop.
2 Thus, the LDF layer is deeper than the layer of UDF for a steep slope. However, the
3 sinking motion above the crest on the gentle slope is diverted to follow the shape of the
4 slope in the upper canopy due to smaller F_{hs} , which is not strong enough to completely
5 penetrate the canopy. As a result, UDF is deeper than the LDF on gentle slopes, in
6 contrast to that on steep slopes. The heterogeneous cooling in the canopy layer causes
7 two baroclinic zones consistent with the UDF and LDF: the upper canopy layer and slope
8 surface layer. The strong baroclinicity on the steep slope surface causes the deep LDF
9 wind to rotate counter-clockwise (i.e., turning upwards on the lower slope, perpendicular
10 to the hill slope). However, the rotated wind is forced to shift down when hitting the top-
11 canopy UDF. The wind at the baroclinic zone with a deep UDF on a gentle slope rotates
12 clockwise, but shifts downslope when hitting the layer of the LDF.

13 **3.3 Turbulent fluxes of momentum and heat**

14 Fig. 7 shows profiles of shear stress $-\overline{u'w'}$. Shear stress is most significant in the
15 region near the top of the canopy where wind impinges on the canopy resulting in strong
16 wind shear. Another region of large shear stress is in the lower canopy. This is related to
17 the wind shifts which lead to strong wind shear. Shear stress is small on the upper slope
18 but increases down the slope. The maximum shear stress at the top of the canopy is
19 located at the wake region (Fig. 7e, f), where the wake vortices are formed. Shear stress is
20 positive above the canopy indicating a downward transfer of momentum that is different
21 from the usually observed downward transport of momentum in the upper canopy. It
22 could be explained by the strong stability above the top of canopy, because strong
23 stability substantially reduces the downward transport of momentum (Mahrt et al., 2000).

1 The momentum transfer is reversed to upward ($-\overline{u'w'} < 0$) when approaching the top of
2 the canopy where airflow is diverted into canopy layer because of the UDF and shear-
3 production of turbulence. Strong upward momentum transfer near the top of canopy on
4 the lower slope is associated with the wake generation behind the hill. In the upper
5 canopy at midslope and downslope, shear stress decays rapidly as z decreases, because of
6 the momentum absorption by the dense crown. The upward momentum ($-\overline{u'w'} < 0$) in
7 the lower canopy indicates momentum sources in the LDF on steep slope. The LDF was
8 recognized as jet-like flow in lower canopy, which has important effects on momentum
9 transfer within canopy (Mao et al., 2007). Upward momentum transport in the canopy is
10 very common, occurring in stable atmospheric conditions (Zhang et al., 2010). The
11 opposite sign in momentum transfer near the slope surface on steep and gentle slope can
12 be explained by the strength of LDF on the slope.

13 The dominant positive turbulent heat flux, $-\overline{w'\theta'}$ indicates downward heat transfer
14 above and within the canopy (Fig. 8). Heat transfer on the upper slope (Fig. 8a, b) is
15 weak because the temperature difference between the canopy and the atmosphere above
16 is small. The downward heat transfer is much stronger on the lower slope, where the air is
17 cooled as a 'cool pool' with the greatest temperature gradient. Turbulent heat flux
18 increases towards the top of the canopy indicating increasing downward heat transfer
19 ($-\overline{w'\theta'} > 0$) but the downward heat transfer decreases in the upper canopy layer. The
20 peak of turbulent heat flux near the top of the canopy is due to the strong radiative
21 cooling in the upper canopy. Below that the near zero and slightly upward turbulent heat
22 flux (Fig. 8) is due to near neutral and negative temperature gradient in the thermal

1 transition zone. As a result of the strong cooling in the ground surface, there are
2 significant downward heat flux transfers in the lower canopy.

3 **3.4 Turbulent Kinetic Energy (TKE) budget**

4 In steady state, the TKE budget Eq. (13) can be written as:

$$0 = T_a + T_t + T_p + P_s + P_b + P_w - \varepsilon \quad (23)$$

5 where T_a is the advection of TKE by the mean wind, T_t represents the turbulent transport
6 of TKE, T_p represents the transport of TKE by pressure perturbation, P_s is the shear
7 production of TKE, P_b is buoyancy production of TKE, P_w is wake production of TKE
8 and ε is viscous dissipation of TKE. We calculate all the terms in the TKE budget
9 equation individually except T_p which is treated as the residual of other terms.

10 TKE is examined to show the intensity of turbulence along the slope (Fig. 9).
11 TKE is usually low within the canopy implying a low turbulence flow under strongly
12 stable atmospheric conditions. TKE is available near the top of canopy on the midslope
13 and downslope. The region with strongly shifting winds is on the lower slope where the
14 wind shear is strong. The largest TKE is found in the region of wake vortices across the
15 canopy edge. The TKE value is larger on the gentle slope than on the steep slope.

16 Contributions from transport and production terms of TKE are complicated. P_b is
17 a principal sink of TKE under stable conditions (Fig. 10 and 11). P_b exhibits negative
18 values near the top of the canopy and slope surface, where flow is stably stratified, which
19 suppresses the turbulence around the top of the canopy and within the deep canopy. In the
20 thermal transition zone, the contribution of P_b is minimal ($P_b \approx 0$ or slightly positive).
21 Buoyancy production is neglected in some studies because P_b is (1) unimportant
22 compared with other terms in TKE budget (Lesnik, 1974) and (2) difficult to measure

1 (Meyers and Baldocchi, 1991), restricting the modeling and measurement studies to near-
2 neutral conditions. Shen and Leclerc (1997) showed that near the top of the canopy, the
3 buoyancy production increases as instability increases, although it is smaller than 10% of
4 shear production in unstable conditions. Leclerc et al. (1990) illustrated a strong positive
5 correlation between buoyancy production and stability ($P_b < 0$) or instability ($P_b > 0$)
6 both within and above the canopy, which is confirmed in our modeling results.

7 Wake production (P_w) is a principal source of TKE in the upper half of the canopy
8 where the canopy is dense (i.e., for large values of a and K_r) on both steep and gentle
9 slopes. Although the magnitude of P_w is very small on a steep slope, the relative
10 contribution of P_w is very large in comparison with other TKE components. Even in the
11 lower canopy layer on the upper slope, P_w is a dominant source of TKE. This unusual
12 phenomenon is induced by the deeper and stronger drainage flow on the slope surface.

13 The positive shear production P_s indicates the net transfer of kinetic energy from
14 the mean flow to the turbulent component of the flow (Fig. 10 and 11). P_s is smaller than
15 P_w except near the top of the canopy, which is consistent with the observations in
16 soybeans (Meyers and Paw U, 1987), deciduous forests (Shi et al., 1987; Meyers and
17 Baldocchi, 1991) and an artificial canopy (Raupach et al., 1987). P_s peaks at the top of
18 the canopy, due to strong wind shear. Shear production is not as important as buoyancy
19 and wake production in the canopy because of strong stability. Observational data also
20 showed that shear production decreases with increasing stability in the lower two-thirds
21 of the canopy (Leclerc et al., 1990).

22 Transport terms are the dominant source to maintain turbulent kinetic energy near
23 the top of the canopy where strong buoyancy suppression occurs (Fig. 10 and 11). TKE is

1 weakly transported by turbulence upward near the canopy top ($T_t < 0$) and downward ($T_t >$
2 0) in the canopy, because turbulence is limited by strong stability above the canopy. TKE
3 transport by advection and turbulence is unimportant at all levels and all slopes in
4 comparison to pressure transport. The field measurement of pressure transport T_p is
5 difficult and the behavior of T_p in the TKE budget is uncertain (Raupach et al., 1996;
6 Finnigan, 2000). Maitani and Seo (1985), Shaw et al. (1990) and Shaw and Zhang (1992)
7 have confirmed that T_p is not small enough to be neglected according to the surface
8 pressure measurements. Pressure diffusion is recognized as an important sink of TKE in
9 the upper canopy and source of TKE below (Dwyer et al., 1997) under unstable
10 conditions. Our results show that the contribution of pressure transport to the overall TKE
11 budget is significant when it is identified as a residual of other TKE components. T_p ,
12 which is of the same order as the production terms, supplies TKE in areas where the
13 buoyancy suppression is very strong and extracts TKE where wake production is
14 dominant. On gentle slopes, T_p is important to compensate the TKE loss by buoyancy
15 near the top of the canopy and in the lower part of the canopy, and compensate TKE gain
16 by wake motion in the upper half of the canopy (Fig. 10). On steep slopes, T_p on the
17 lower half of the slope plays the same role as on gentle slopes to compensate the TKE
18 loss by buoyancy and gain by wake (Fig. 11d-f), but the relative significance of wake
19 production becomes more prominent. On the upper slope (Fig. 11a-c), pressure transport
20 is important in the whole canopy to work against wake production. Our results suggest
21 that the pressure perturbation is stronger compared with other terms on steep slopes. In
22 addition, thermal effects on the upper steep slope are diminished and the canopy effect is

1 magnified since the air is warm and the temperature gradient is small on the elevated
2 topography.

3 **4 Concluding remarks**

4 Stably stratified canopy flows in complex terrain are investigated by a RNG
5 turbulent model, with emphasis on strong boundary effects, including persistent thermal
6 forcing from ground and canopy elements, damping force from canopy drag elements,
7 and buoyancy effects from temperature stratification and topographic character.

8 The fundamental characteristics of nighttime canopy flow over complex terrain
9 are addressed by this numerical simulation as follows:

10 **(1) Multiple layering of thermal stratification** The stability around the canopy is
11 characterized by stratification with super stable layers above the top of the canopy and in
12 the lower canopy, and an unstable layer within the canopy (Fig. 2, 3, 4).

13 **(2) Bifurcation of thermal-driven drainage flows** The drainage flow above the canopy
14 is mainly driven by thermal stratification, being separated into two streams in the canopy:
15 the upper-canopy drainage flow (UDF) layer and the lower-canopy drainage flow (LDF)
16 layer (Fig. 1, 5, 6).

17 **(3) Buoyancy suppression of turbulence** The downward transport of momentum and
18 heat flux in the canopy is reduced due to strong stability and reversed to be upward in the
19 deep canopy (Fig. 7, 8). Buoyancy production suppresses turbulence significantly near
20 the top of the canopy and in the deep canopy (Fig. 10, 11).

21 The thermal stratification and nocturnal drainage flows are interactive. The
22 drainage flows, initiated by thermal stratification, result in the formation of super stable

1 layers. In addition, the drainage flows intensify the temperature inversion down the slope,
2 thus intensifying the stability of super stable layers. The properties of momentum and
3 heat transfer may be related to the ‘shear-driven’ and ‘buoyancy-driven’ coherent
4 structures that can lead to decoupling between the lower and upper canopy (Dupont et al.,
5 2012). *Although* unstable layer is more likely to occur during the foliated period (Dupont
6 et al., 2012) and may only have influence on the small-scale motions within the canopy
7 (Jacob et al., 1992), the super-stable layers associated with flow decoupling have direct
8 influence on a larger scale soil, within- and above-canopy exchange processes
9 (Alekseychik, et al., 2013).

10 The canopy flow behavior presented in Fig.1 is expected to be measurable
11 directly by multiple eddy-flux towers that are equipped with multi-level
12 micrometeorological instruments (Feigenwinter et al., 2010; Baldocchi, 2008). Some
13 turbulent exchange processes remain uncertain and require further study, including (i)
14 how the varied vegetation structure, strength of background wind and ambient stability
15 influence the within-canopy stratification and turbulence, and (ii) how the complicated
16 flows regulate scalar transfer within the canopy and scalar exchange between the
17 vegetation and atmosphere aloft.

18

19

20

21

22

1

2 **Acknowledgements**

3 This research was supported, in part, under National Science Foundation Grants ATM-
4 0930015, CNS-0958379 and CNS-0855217, PSC-CUNY Research Awards (Enhanced)
5 ENHC-42-64, and the City University of New York High Performance Computing
6 Center. C.Y. is grateful to the International Meteorological Institute for supporting him as
7 a Rossby Fellow to complete this work.

8

1 **References**

- 2 Alekseychik, I. Mammarella, P., Launiainen, S., Rannik, Ü., Vesala, T.: Evolution of the
3 nocturnal decoupled layer in a pine forest canopy. *Agric. For. Meteor.* 174-175, 15-27,
4 2013.
- 5 Aubinet, M., Feigenwinter, C.: Direct CO₂ advection measurements and the night flux
6 problem. *Agric. For. Meteor.* 150, 651-654, 2010.
- 7 Aubinet, M., Heinesch, B., Yernaux, M.: Horizontal and vertical CO₂ advection in a
8 sloping forest. *Bound.-Layer Meteor.* 108, 397–417, 2003.
- 9 Baldocchi, D. D.: 'Breathing' of the terrestrial biosphere: lessons learned from a global
10 network of carbon dioxide flux measurement systems. *Austral. J. Bot.* 56, 1-26, 2008.
- 11 Baldocchi, D. D., and Meyers, T. P.: Turbulence structure in a deciduous forest. *Bound.-*
12 *Layer Meteor.* 43, 345-364, 1998.
- 13 Basu, S., and Porté-Agel, F.: Large-eddy simulation of stably stratified atmospheric
14 boundary layer turbulence. a scale dependent dynamic modeling approach. *J. Atmos. Sci.*
15 63, 2074-2091, 2006.
- 16 Basu, S., Porté -Agel, F., Fofoula-Georgiou, E., Vinuesa, J. F., Pahlow, M.: Revisiting
17 the local scaling hypothesis in stably stratified atmospheric boundary-layer turbulence. an
18 integration of field and laboratory measurements with large-eddy simulations. *Bound.-*
19 *Layer Meteor.* 119, 473–500, 2006.
- 20 Basu, S., Bosveld, F.C., Holtslag, A. A. M.: Stable boundary layers with low-level jets.
21 what did we learn from the LES intercomparison within GABLS3? The fifth international
22 symposium on computational wind engineering (CWE2010) Chapel Hill, NC, USA, May
23 23-27, 2010.
- 24 Belcher, S. E., Finnigan, J. J., Harman, I. N.: Flows through forest canopies in complex
25 terrain. *Ecol. Appl.* 18, 1436-1453, 2008.
- 26 Bergen, J. D.: Vertical profiles of wind speed in a pine stand. *For. Sci.* 17, 314-322, 1971.
- 27 Biswas, G., Eswaram V., Eds: Turbulent flows: Fundamentals, experiments and modeling,
28 Narosa, 256pp, 2002.
- 29 Brost, R. A., Wyngaard, J. C.: A model study of the stably stratified planetary boundary
30 layer. *J. Atmos. Sci.* 35, 1427-1440, 1978.
- 31 Burns, S. P., Sun, J., Lenschow, D. H., Oncley, S. P., Stephens, B. B., Yi C., Anderson, D.
32 E., Hu, J., Monson, R. K.: Atmospheric stability effects on wind fields and scalar mixing
33 within and just above a subalpine forest in sloping terrain. *Bound.-Layer Meteor.* 138,
34 231-262, 2011.
- 35 Chen, H., Yi, C.: Optimal control of katabatic flows within canopies. *Q. J. Roy. Meteor.*
36 *Soc.* DOI: 10.1002/qj.1904, 2012.
- 37 Coceal, O., Thomas, T. G., Castro, I. P., Belcher, S. E.: Mean flow and turbulence
38 statistics over groups of urban-like cubical obstacles. *Bound.-Layer Meteor.* 121, 49-519,
39 2006.

- 1 Cruz, M. G., Alexander, M. E., Walimoto, R. H.: Development and testing of models for
2 predicting crown fire rate of spread in conifer forest stands, *Can. J. For. Res.* 35, 1626-
3 1639, 2005.
- 4 Denmead, O. T., Bradley, E. F.: Flux-gradient relationships in a forest canopy, in *The*
5 *Forest-Atmosphere Interaction*, edited by B. A. Hutchison and B. B. Hicks, pp. 421–442,
6 D. Reidel, Dordrecht, 1985.
- 7 Dupont, S., Brunet, Y., Finnigan, J. J.: Large-eddy simulation of turbulent flow over a
8 forested hill: validation and coherent structure identification. *Q. J. Roy. Meteor. Soc.* 134,
9 1911-1929, 2008.
- 10 Dupont, S., F. Gosselin, PY, C., De Langere, E., Hemon, P., Brunet, Y.: Modeling
11 waving crops using large-eddy simulation: comparison with experiments and a linear
12 stability analysis. *J. Fluid Mech.* 652, 5-44, 2010.
- 13 Dupont, S., Patton, E. G.: Momentum and scalar transport within a vegetation canopy
14 following atmospheric stability and seasonal canopy changes: the CHATS experiment.
15 *Atmos. Chem. Phys.* 12, 5913-5935, 2012.
- 16 Dwyer, M. J., Patton, E. G., Shaw, R. H.: Turbulent kinetic energy budgets from a large-
17 eddy simulation of airflow above and within a forest canopy. *Bound.-Layer Meteor.* 84,
18 23-43, 1997.
- 19 Edburg, S. L., Allwine, G., Lamb, B., Stock, D., Thistle, H., Peterson, H., Strom, B.: A
20 simple model to predict scalar dispersion within a successively thinned loblolly pine
21 canopy. *J. Appl. Meteor. Climatol.* 49, 1913–1926, 2010.
- 22 Feigenwinter, C., Montagnani, L., Aubinet, M.: Plot-scale vertical and horizontal
23 transport of CO₂ modified by a persistent slope wind system in and above an alpine
24 forest. *Agric. For. Meteor.* 150, 665–673, 2010.
- 25 Finnigan, J. J.: Turbulence in plant canopies. *Annu. Rev. Fluid Mech.* 32, 519-571, 2000.
- 26 Finnigan, J. J., Belcher, S. E.: Flow over a hill covered by a plant canopy. *Q. J. Roy.*
27 *Meteor. Soc.* 130:1–29, 2004.
- 28 Fons, R. G.: Influence of forest cover on wind velocity. *J. For.* 38, 481-486, 1940.
- 29 Galperin, B., Orszag, S. A.: *Large Eddy Simulation of Complex Engineering and*
30 *Geophysical Flows*. Cambridge University Press, 622 pp, 1993.
- 31 Goulden, M. L., Munger, J. W., Fan, S. M., Daube, B. C., Wofsy, S. C.: Measurements of
32 carbon sequestration by long-term eddy covariance: methods and a critical evaluation of
33 accuracy, *Global Change Biol.* 2, 169-182, 1996.
- 34 Graham, J., Meneveau, C.: Modeling turbulent flow over fractal trees using renormalized
35 numerical simulation: Alternate formulations and numerical experiments. *Phys. Fluids* 24,
36 125105, 2012.
- 37 Gross G.: *Numerical Simulation of Canopy Flows*. In: Douglas J, Marcus M (eds)
38 Springer, Berlin, 167 pp, 1993.
- 39 Hoerner S. F.: *Fluid dynamic drag: practical information on aerodynamic drag and*
40 *hydrodynamic resistance*. Midland Park, NJ, 1965.

- 1 Huang, J., Cassiani, M., Albertson, J. D.: The effects of vegetation density on coherent
2 turbulent structures within the canopy sublayer: A large-eddy simulation study, *Bound.-*
3 *Layer Meteor.* 133, 253–275, 2009.
- 4 Jackson, P. S., Hunt, J. C. R.: Turbulent wind flow over a low hill, *Q. J. Roy. Met. Soc.*
5 101, 929-99, 1975.
- 6 Jacobs, A.F.G., van Boxel, J.H., Shaw, R.H.: The dependence of canopy layer turbulence
7 on within-canopy thermal stratification. *Agric. For. Meteor.* 58: 247-256,1992.
- 8 Janssens, I. A., Lankreijer, H., Matteucci, G., Kowalski, A. S., Buchmann, N., Epron, D.,
9 Pilegaard, K., Kutsch, W., Longdoz, B., Grünwald, T., Montagnani, L., Dore, S.,
10 Rebmann, C., Moors, E. J., Grelle, A., Rannik, Ü., Morgenstern, K., Oltchev, S., Clement,
11 R., Gudmundsson, J., Minerbi, S., Berbigier, P., Ibrom, A., Moncrieff, J., Aubinet, M.,
12 Bernhofer, C., Jensen, N. O., Vesala, T., Granier, A., Schulze, E. D., Lindroth, A.,
13 Dolman, A. J., Jarvis, P. G., Ceulemans, R., Valentini, R.: Productivity overshadows
14 temperature in determining soil and ecosystem respiration across European forests. *Glob.*
15 *Chang. Biol.* 7, 269–278, 2001.
- 16 Katul, G. G., Finnigan, J. J., Poggi, D., Leuning, R., Belcher, S. E.: The influence of hilly
17 terrain on canopy-atmospheric carbon dioxide exchange. *Bound.-Layer Meteor.* 118,189-
18 216, 2006.
- 19 Kim, H. G., Patel, V. C.: Test of turbulence models for wind flow over terrain with
20 separation and recirculation. *Bound.-Layer Meteor.* 94, 5-21, 2000.
- 21 Lalic, B., Mihailovic, D. T.: A new approach in parameterization of momentum transport
22 inside and above forest canopy under neutral conditions. *Integrated Assessment and*
23 *Decision Support, Proceedings of the 1st biennial meeting of the International*
24 *Environmental Modelling and Software Society, Switzerland, iEMSs, Manno, 139-154,*
25 2002.
- 26 Landsberg J. J., James, G. B.: Wind profiles in plant canopies: studies on an analytical
27 model. *J. Appl. Ecol.* 8, 729-741, 1971.
- 28 Leclerc, M. Y., Beissner, K. C., Shaw, R. H., den Hartog, G., Neumann, H. H.: The
29 influence of atmospheric stability on the budgets of the reynolds stress and turbulent
30 kinetic energy within and above a deciduous forest. *J. Appl. Meteor.* 29, 916–933, 1990.
- 31 Lemon, E., Allen, L. H., and Muller, L.: Carbon dioxide exchange of a tropical rain forest.
32 2. *BioScience* 20, 1054–1059, 1970.
- 33 Lesnik, G. E.: Results of measurement of turbulent energy balance components in a layer
34 of vegetation. *Izv. Atmos. Oceanic Phys.* 10, 652–655, 1974.
- 35 Mahrt, L.: Momentum Balance of Gravity Flows. *J. Atmos. Sci.* 39, 2701– 2711, 1982.
- 36 Mahrt, L., Lee, X., Black, A., Neumann, H., Staebler, R. M.:Nocturnal mixing in a forest
37 subcanopy. *Agric. For. Meteor.* 101, 67-78, 2000.
- 38 Maitani, T., Seo, T.: Estimates of velocity-pressure and velocity-pressure gradient
39 interactions in the surface layer over plant canopies. *Bound.-Layer Meteor.* 33, 51–60,
40 1985.

- 1 Mao, S., Feng, Z., Michaelides, E. E.: Large-eddy simulation of low-level jet-like flow in
2 a canopy. *Environ. Fluid Mech.* 7, 73-93, 2007.
- 3 Mao, S., Leclerc, M.Y., Michaelides, E.E.: Passive scalar flux footprint analysis over
4 horizontally inhomogenous plant canopy using large-eddy simulation. *Atmos. Environ.*
5 42, 5446-5458, 2008.
- 6 Meyers, T.P., Baldocchi, D. D.: The budgets of turbulent kinetic energy and Reynolds
7 stress within and above deciduous forest. *Agric. For. Meteor.* 53, 207-222, 1991.
- 8 Meyers, T.P., Paw U, K.T.: Testing of a higher-order closure model for modeling airflow
9 within and above plant canopies. *Bound.-Layer Meteor.* 37, 297–311, 1986.
- 10 Montagnani, L., Manca G., Canepa, E., Georgieva, E., Acosta, M., Feigenwinter, C.,
11 Janous, D., Kerschbaumer, G., Lindroth, A., Minach, L., Minerbi, S., Mölder, m.,
12 Pavelka, M., Seufert, G., Zeri, M., Ziegler, W.: A new mass conservation approach to the
13 study of CO₂ advection in an alpine forest. *J. Geophys. Res.* 114, D07306.
14 doi:10.1029/2008JD010650, 2009.
- 15 Oliver, H. R.: Wind profiles in and above a forest canopy. *Q. J. Roy. Meteor. Soc.* 97,
16 548, 1971.
- 17 Pattanapol, W., Wakes, S. J., Hilton, M. J., Dickinson, K. J. M.: Modeling of surface
18 roughness for flow over a complex vegetated surface. *World Acad. Sci. Eng. Technol.* 26,
19 271-291, 2006.
- 20 Pinard, J., and Wilson, J. D.: First- and second-order closure models for wind in a plant
21 canopy. *J. Appl. Meteor.* 40, 1762-1768, 2001.
- 22 Poggi D., Katul, G. G.: The ejection-sweep cycle over gentle hills covered with bare and
23 forested surfaces. *Bound.-Layer Meteor.* 122, 493-515, 2007a.
- 24 Poggi D., Katul, G. G.: An experimental investigation of the mean momentum budget
25 inside dense canopies on narrow gentle hilly terrain. *Agric. For. Meteor.* 144:1–13,
26 2007b.
- 27 Queck, R., Bernhofer, C.: Constructing wind profiles in forests from limited
28 measurements of wind and vegetation structure. *Agric. For. Meteor.* 150, 724-735, 2010.
- 29 Raupach, M. R.: A Lagrangian analysis of scalar transfer in vegetation canopies. *Q. J.*
30 *Roy. Meteor. Soc.* 113, 107-130, 1987.
- 31 Raupach, M. R., Finnigan, J. J., Brunet, Y.: Coherent eddies and turbulence in vegetation
32 canopies: The mixing-layer analogy. *Bound.-Layer Meteor.* 78, 351-382, 1996.
- 33 Ross, A. N.: Large-eddy simulation of flow over forested ridges. *Bound.-Layer Meteor.*
34 128, 59–76, 2008.
- 35 Ross, A. N., Vosper, S. B.: Neutral turbulent flow over forested ridges. *Q. J. Roy. Meteor.*
36 *Soc.* 131, 1841-1862, 2005.
- 37 Schaeffer, S. M., Miller, J. B., Vaughn, B. H., J. White, W. C., Bowling, D.R.: Long-term
38 field performance of a tunable diode laser absorption spectrometer for analysis of carbon
39 isotopes of CO₂ in forest air. *Atmos. Chem. Phys. Discuss.* 83, 9531–9568, 2008.
- 40 Schlichting, H.: *Boundary Layer Theory*. 4th ed., McGraw-Hill, 647 pp, 1960.

- 1 Shaw, R. H.: Secondary wind speed maxima inside plant canopies. *J. Appl. Meteor.* 16,
2 514-521, 1977.
- 3 Shaw, R. H., Zhang, X. J.: Evidence of pressure-forced flow in a forest, *Bound.-Layer*
4 *Meteor.* 58, 47–64, 1992.
- 5 Shaw, R. H., Paw U, K. T., Zhang, X. J., Gao, W., Den Hartog, G., Neumann, H. H.:
6 Retrieval of turbulent pressure fluctuations at the ground surface beneath a forest,
7 *Bound.-Layer Meteor.* 50, 319–338, 1990.
- 8 Shen, S., Leclerc, M. Y.: Modeling the turbulence structure in the canopy layer, *Agric.*
9 *For. Meteor.* 87, 3-25, 1997.
- 10 Shi, G., Shaw, R. H., Thurtell, G.W., den Hartog, G., Neumann, H. H.: The turbulent
11 kinetic energy budget within and above a deciduous forest. 18th Conf. on Agric. and For.
12 *Meteor.*, Boston, Amer. Meteor. Soc. 187-188, 1987.
- 13 Siebicke, L., Hunner, M., Foken, T.: Aspects of CO₂ advection measurements, *Theor.*
14 *Appl. Climatol.* 109, 109–131, 2012.
- 15 Smith, L.M., Reynolds, W. C.: On the Yaghot-Orszag Renormalization group method for
16 deriving turbulence statistics and models. *Phys. Fluids A* 4, 364, 1992.
- 17 Staebler, R. M., Fitzjarrald D. R.: Observing subcanopy CO₂ advection. *Agric. For.*
18 *Meteor.* 12, 139-156, 2004.
- 19 Stoll R, Porté-Agel, F.: Large-eddy simulation of the stable atmospheric boundary layer
20 using dynamic models with different averaging schemes. *Bound.-Layer Meteor.* 126, 1-
21 28, 2008.
- 22 Sun, J., Burns, S. P., Delany, A. C., Oncley, S. P., Turnipseed, A. A., Stephens, B. B.,
23 Lenschow, D. H., LeMone, M. A., Monson, R. K., Anderson, D. E.: CO₂ transport over
24 complex terrain. *Agric. For. Meteor.* 145, 1–21, 2007.
- 25 Sypka, P., Starzak, R.: Simplified, empirical model of wind speed profile under canopy
26 of Istebna spruce stand in mountain valley. *Agric. For. Meteor.* 171-172, 220-233, 2013.
- 27 Tennekes, T., Lumley, J. L.: A first course in turbulence. MIT, Cambridge, MA, 300 pp,
28 1972.
- 29 Tóta, J., Fitzjarrald, D. R., da Silva Dias, M. A. F.: Amazon rainforest exchange of
30 carbon and subcanopy air flow Manaus LBA site- a complex terrain condition. *The*
31 *Scientific World J.* 165067.doi:10.1100/2012/165067, 2012.
- 32 Turnipseed, A. A., Anderson, D. E., Blanken, P. D., Baugh, W. M., Monson, R. K.:
33 Airflows and turbulent flux measurements in mountainous terrain Part 1. Canopy and
34 local effects. *Agric. For. Meteor.* 119, 1–21, 2003.
- 35 van Gorsel, E., Harman, I. N., Finnigan, J. J., Leuning, R.: Decoupling of air flow above
36 and in plant canopies and gravity waves affect micrometeorological estimates of net
37 scalar exchange. *Agric. For. Meteor.* 151, 927-933, 2011.
- 38 von Kármán, T.: Mechanische Ähnlichkeit and yurbulenz. *Nachr Ges Wiss Göttingen*
39 *Math Phys. Kl* 68, 58–76, 1930.

1 Wang, W.: The influence of topography on single-tower-based flux measurement under
2 unstable condition: a modeling perspective. *Theor. Appl. Climatol.* 99, 125-138, 2010.

3 Wang, W., Yi, C.: A new nonlinear analytical model for canopy flow over a forested hill.
4 *Theor. Appl. Climatol.* 109, 549-563, 2012.

5 Wilson, J. D., Finnigan, J. J., Raupach, M. R.: A first-order closure for disturbed plant-
6 canopy flows, and its application to winds in a canopy on a ridge. *Q. J. Roy. Meteor. Soc.*
7 124, 705-732, 1998.

8 Wolfe, G. M., Thornton, J. A., McKay, M., Goldstein, A. H.: Forest-atmosphere
9 exchange of ozone: sensitivity to very reactive biogenic VOC emissions and implications
10 for in-canopy photochemistry. *Atmos. Chem. Phys.* 11, 7875-7891, 2011.

11 Xu., X., Yi C.: The influence of geometry on recirculation and CO₂ transport over
12 forested hills. *Meteorol. Atmos. Phys.* 119, 187-196, 2013.

13 Yakhot, V., Orszag S. A.: Renormalization group analysis of turbulence: basic theory. *J.*
14 *Sci. Comput.* 1, 3-61, 1986a.

15 Yakhot, V., Orszag, S. A.: Renormalization group analysis of turbulence. *Phys. Rev. Lett.*
16 57, 1722-1724, 1986b.

17 Yakhot, V., Orszag, S. A., Thangam, S., Gatski, T. B., Speziale, C. G.: Development of
18 turbulence models for shear flows by a double expansion technique. *Phys. of Fluids A* 4,
19 1510-1520, 1992.

20 Yi, C., Monsoon, R. K., Zhai, Z., Anderson, D. E., Lamb, B., Allwine, G., Turnipseed,
21 A. A., Burns, S. P.: Modeling and measuring the nocturnal drainage flow in a high-
22 elevation, subalpine forest with complex terrain. *J. Geophys. Res.* 110, D22303.
23 doi:10.1029/2005JD006282, 2005.

24 Yi, C.: Momentum transfer within canopies. *J. Appl. Meteor Climatol.* 47, 262- 275,
25 2008.

26 Yi, C., Anderson, D. E., Turnipseed, A. A., Burns, S. P., Aparks, J. P., Stannard, D. I.,
27 Monson, R. K.: The contribution of advective fluxes to net ecosystem exchange in a
28 high-elevation, subalpine forest. *Ecol. Appl.* 18, 1379-1390, 2008.

29 Zängl, G.: The impact of upstream blocking, drainage flow and the geostrophic pressure
30 gradient on the persistence of cold-air pools. *Q. J. R. Meteorol. Soc.* 129, 117-137, 2003.

31 Zhang, G., Leclerc, M. Y., Karipot, A.: Local flux-profile relationships of wind speed and
32 temperature in a canopy layer in atmospheric stable conditions. *Biogeosciences* 7, 3625-
33 3636, 2010.

34
35
36

1 List of illustrations

2 Figure 1. Simulated streamlines in the forested hill: (a) $H/L = 0.6$; (b) $H/L = 1.0$. The
3 translucent green masks indicate the regimes with instability within canopy. The top of
4 canopy is marked by back dashed line. The black ‘WV’ marks the region of wake
5 vortices next to the edge of canopy. The ‘DS’ in (a) and ‘UD’ in (b) indicate the region of
6 down-sweep wind and up-draft wind on the gentle and steep slopes, respectively.

7 Figure 2. Contours of potential temperature (K) along the right slope: (a) $H/L = 0.6$; (b)
8 $H/L = 1.0$. The difference between isotherms is 0.25 K. The numbers on isotherms
9 indicate the temperature. The x-axis is normalized by the half length scale of the hill L
10 and y-axis is normalized by the height of the canopy h . White dashed lines indicate the
11 top of canopy and the isotherms marked with cyan blue dashed lines highlight the ‘fish-
12 head’ temperature distribution.

13 Figure 3. Potential temperature (K) profiles on the slope for $H/L = 0.6$ (blue) and $H/L =$
14 1.0 (red). The locations of the six sections are labeled as a-f, and their locations with
15 respect to the hill are presented. Horizontal distances are normalized by the half length
16 scale L of the hill. The cyan blue curves indicate the thermal transition zone with negative
17 temperature gradient.

18 Figure 4. Locations of super stable layers for $H/L = 0.6$ and $H/L = 1.0$ (left panel). The
19 primary super stable layers are marked by dash-dotted lines with yellow solid circles and
20 secondary super stable layers are marked by dash-dotted lines with green solid circles.
21 The Ri numbers at locations indicated by the yellow and green solid circles are extremely
22 large, which are illustrated on the right panel for the locations (b) and (e). PSL denotes
23 primary super stable layer. SSL denotes secondary super stable layer. UL denotes
24 unstable layer.

25 Figure 5. Profiles of streamwise velocity (u , m s^{-1} , top panel) and vertical velocity (w , m
26 s^{-1} , bottom panel) for $H/L = 0.6$ (blue) and $H/L = 1.0$ (red). The locations of the six
27 sections are labeled as a-f, and their locations with respect to the hill are marked in Fig. 3
28 with the same letters. Note that wind velocity on the slope surface is not zero because the
29 centers of bottom grid cells in the numerical calculation are not exactly at the surface.

30 Figure 6. Wind velocity (U , m s^{-1}) on the slopes for (a) $H/L = 0.6$ and (b) $H/L = 1.0$. The
31 white solid lines are streamlines as shown in Figure 1. The black-white dashed lines
32 denote the top of the canopy.

33

- 1 Figure 7. Profiles of shear stress, $-\overline{u'w'}$ ($10^{-3} \text{ m}^2 \text{ s}^{-2}$) on the slope for $H/L = 0.6$ (blue) and
2 $H/L = 1.0$ (red). The locations of the six sections are labeled as a-f, and their locations
3 with respect to the hill are marked in Fig. 3 with the same letters.
- 4 Figure 8. Profiles of turbulent Heat Flux, $-\overline{w'\theta'}$ ($10^{-2} \text{ K m s}^{-1}$) on the slope for $H/L = 0.6$
5 (blue) and $H/L = 1.0$ (red). The locations of the six sections are labeled as a-f, and their
6 locations with respect to the hill are marked in Fig. 3 with the same letters.
- 7 Figure 9. Contours of turbulent kinetic energy ($\text{m}^2 \text{ s}^{-2}$): (a) $H/L = 0.6$; (b) $H/L = 1.0$. The
8 black dashed lines indicate the top of canopy.
- 9 Figure 10. Profiles of TKE components ($10^{-3} \text{ m}^2 \text{ s}^{-3}$) for $H/L = 0.6$. T_a is the advection of
10 TKE by the mean wind, T_t represents the turbulent transport of TKE, T_p represents the
11 transport of TKE by pressure perturbation, P_s is the shear production of TKE, P_b is
12 buoyancy production of TKE, P_w is wake production of TKE and ϵ is viscous dissipation
13 of TKE. The locations of the six sections are labeled as a-f, and their locations with
14 respect to the hill are marked in Fig. 3 with the same letters.
- 15 Figure 11. The same as in Fig. 10, but for $H/L = 1.0$.
- 16
- 17

1
2

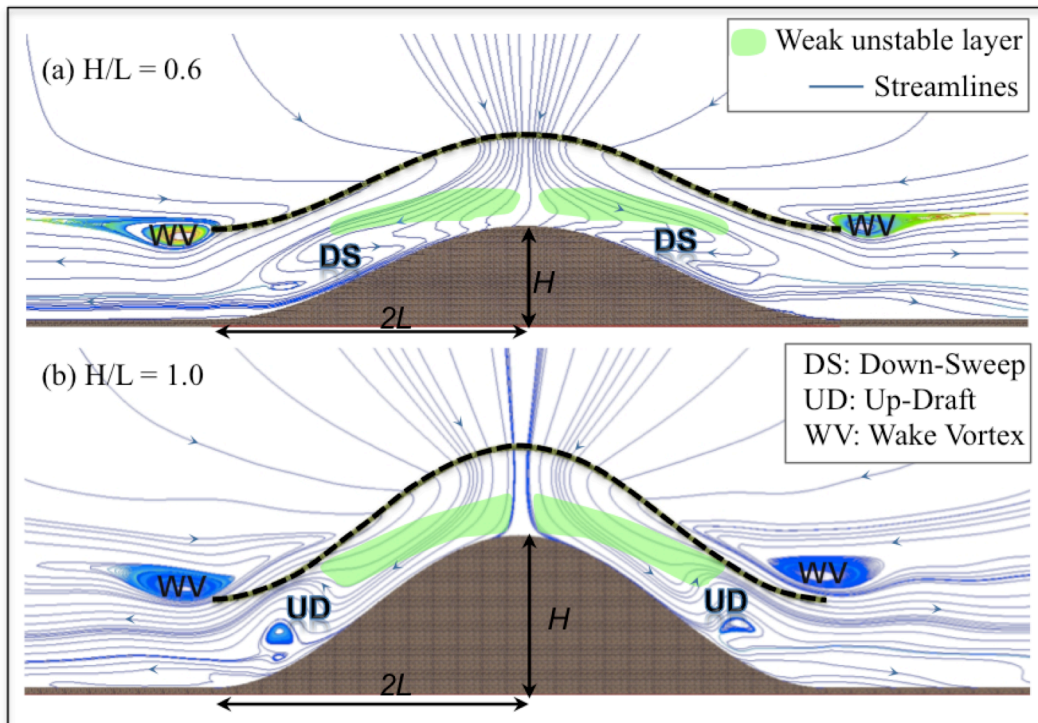


Figure 1. Simulated streamlines in the forested hill: (a) $H/L = 0.6$; (b) $H/L = 1.0$. The translucent green masks indicate the regimes with instability within canopy. The top of canopy is marked by back dashed line. The black 'WV' marks the region of wake vortices next to the edge of canopy. The 'DS' in (a) and 'UD' in (b) indicate the region of down-sweep wind and up-draft wind on the gentle and steep slopes, respectively.

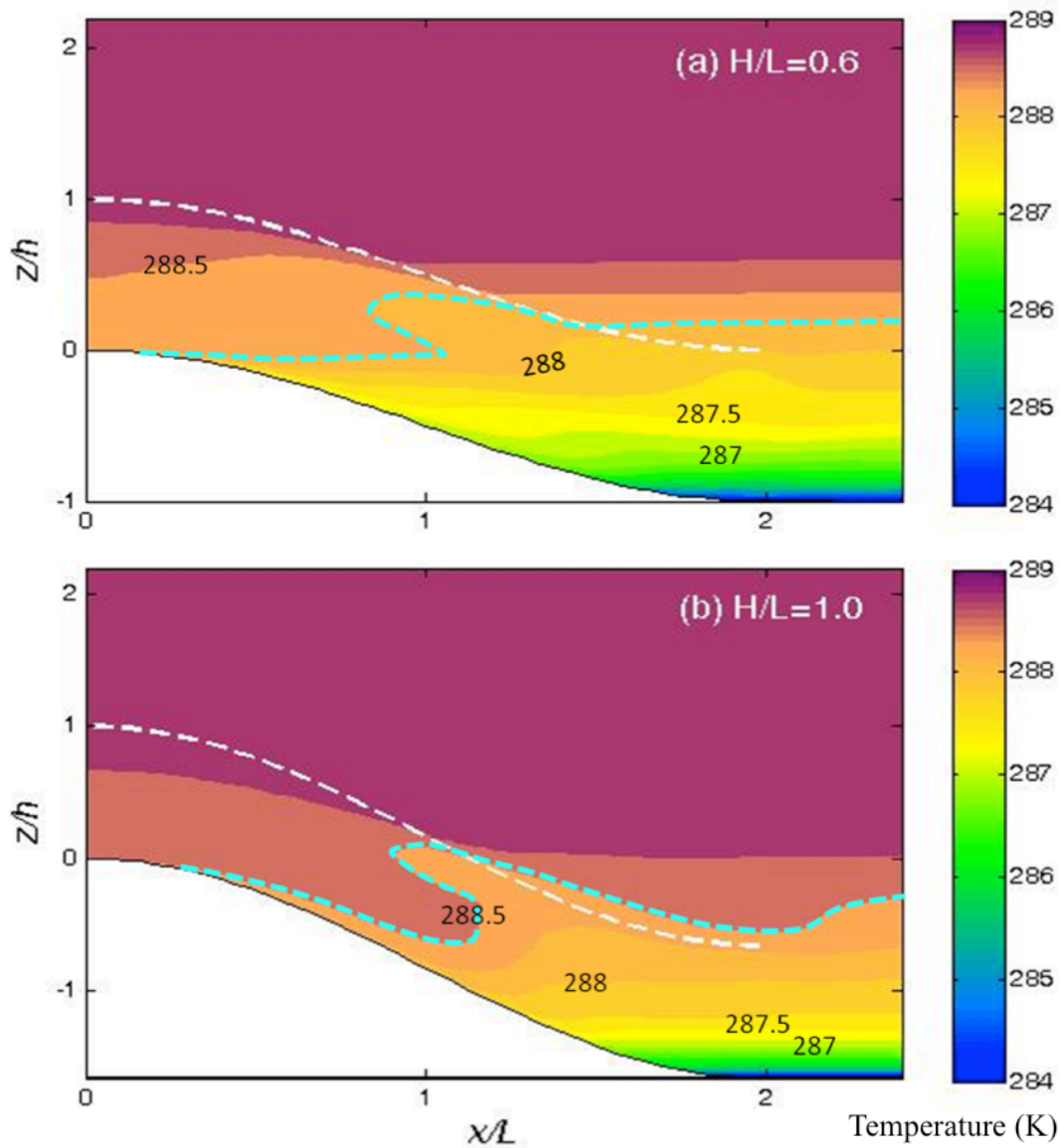


Figure 2. Contours of potential temperature (K) along the right slope: (a) $H/L = 0.6$; (b) $H/L = 1.0$. The difference between isotherms is 0.25 K. The numbers on isotherms indicate the temperature. The x-axis is normalized by the half length scale of the hill L and y-axis is normalized by the height of the canopy h . White dashed lines indicate the top of canopy and the isotherms marked with cyan blue dashed lines highlight the 'fish-head' temperature distribution.

1

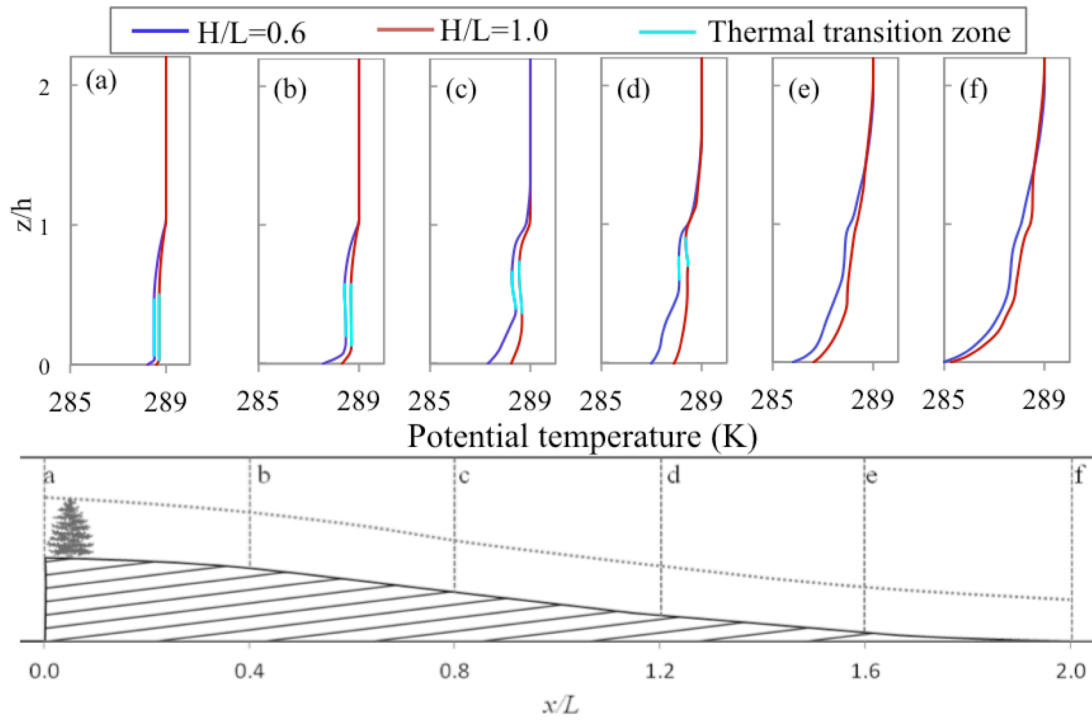


Figure 3. Potential temperature (K) profiles on the slope for $H/L = 0.6$ (blue) and $H/L = 1.0$ (red). The locations of the six sections are labeled as a-f, and their locations with respect to the hill are presented. Horizontal distances are normalized by the half length scale L of the hill. The cyan blue curves indicate the thermal transition zone with negative temperature gradient.

2

1

2

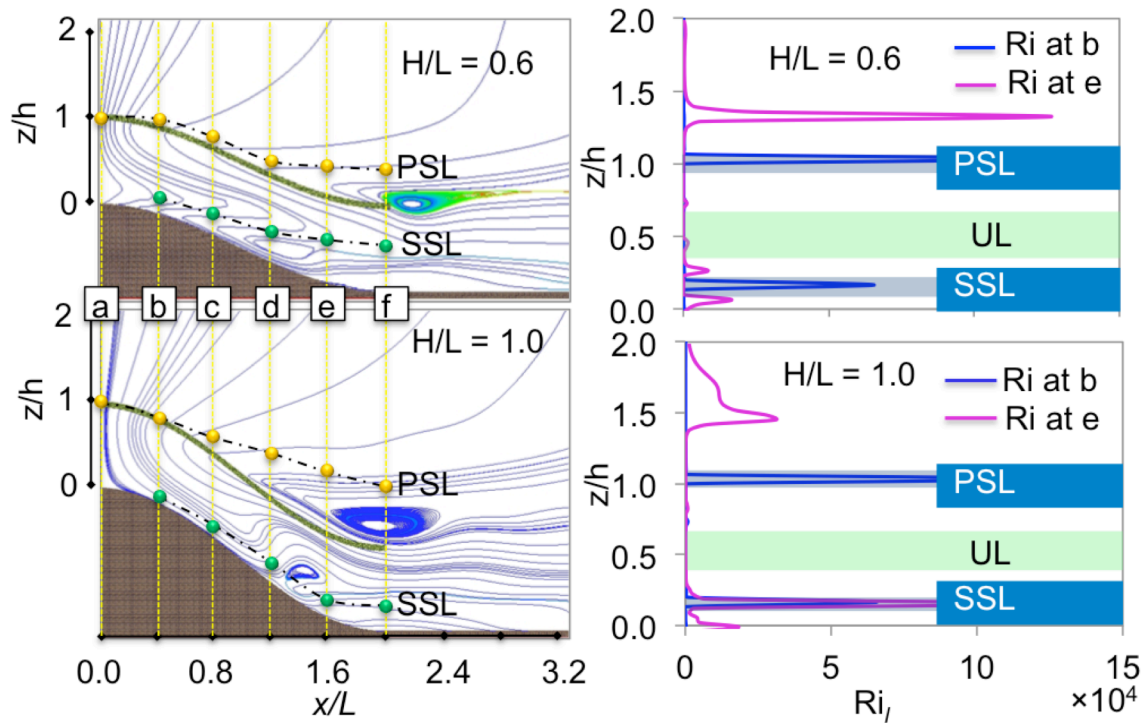


Figure 4. Locations of super stable layers for $H/L = 0.6$ and $H/L = 1.0$ (left panel). The primary super stable layers are marked by dash-dotted lines with yellow solid circles and secondary super stable layers are marked by dash-dotted lines with green solid circles. The Ri numbers at locations indicated by the yellow and green solid circles are extremely large, which are illustrated on the right panel for the locations (b) and (e). PSL denotes primary super stable layer. SSL denotes secondary super stable layer. UL denotes unstable layer.

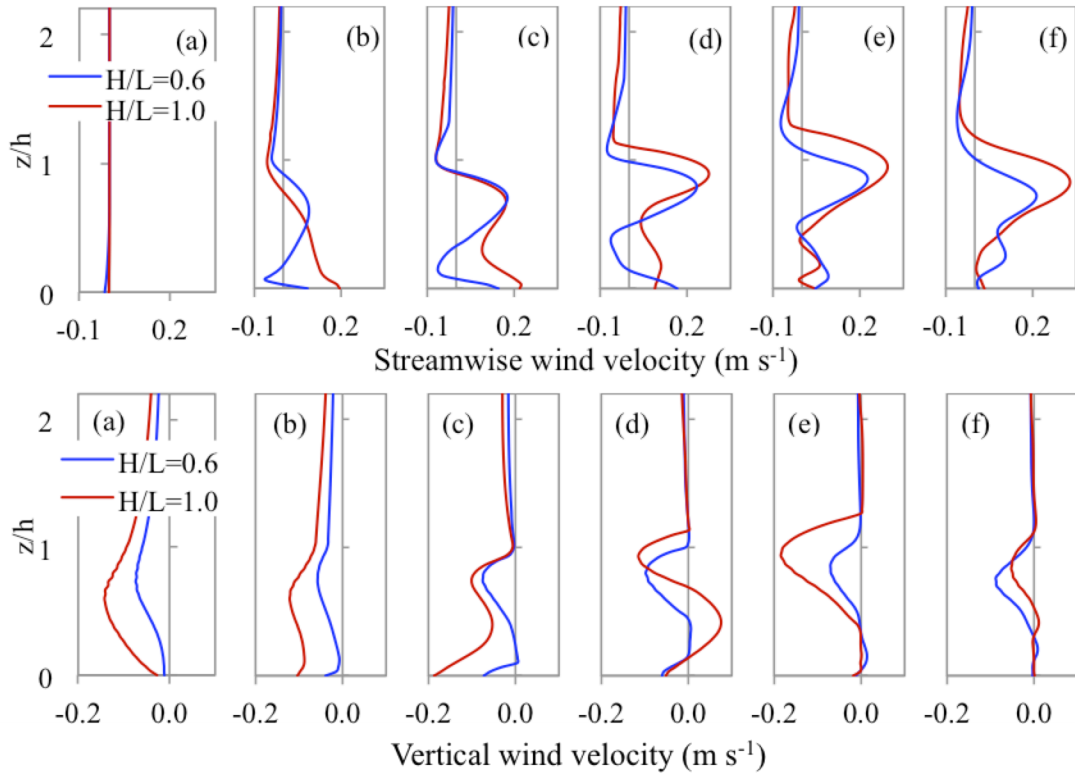


Figure 5. Profiles of streamwise velocity (u , m s^{-1} , top panel) and vertical velocity (w , m s^{-1} , bottom panel) for $H/L = 0.6$ (blue) and $H/L = 1.0$ (red). The locations of the six sections are labeled as a-f, and their locations with respect to the hill are marked in Fig. 3 with the same letters. Note that wind velocity on the slope surface is not zero because the centers of bottom grid cells in the numerical calculation are not exactly at the surface.

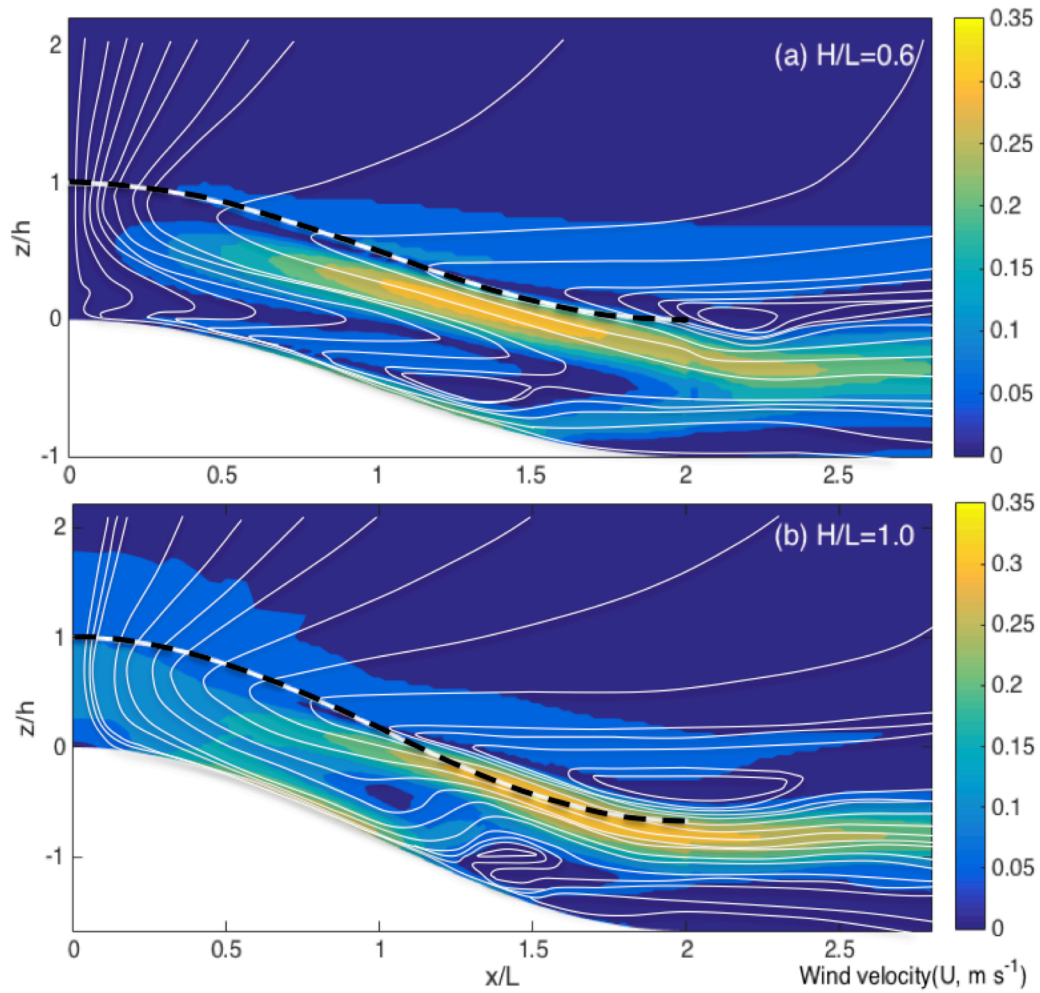


Figure 6. Wind velocity (U , m s^{-1}) on the slopes for (a) $H/L = 0.6$ and (b) $H/L = 1.0$. The white solid lines are streamlines as shown in Figure 1. The black-white dashed lines denote the top of the canopy.

1

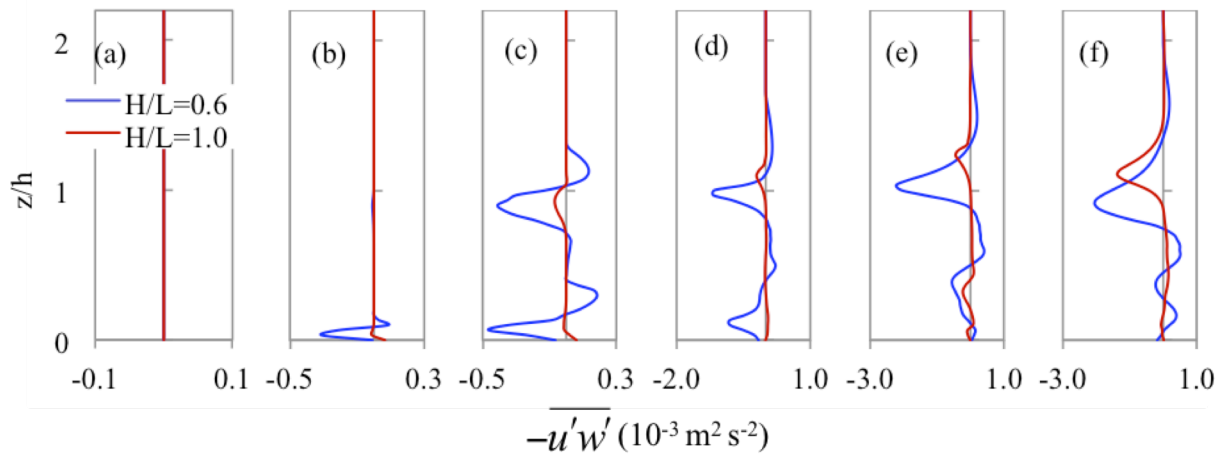


Figure 7. Profiles of shear stress, $-\overline{u'w'}$ ($10^{-3} \text{ m}^2 \text{ s}^{-2}$) on the slope for $H/L = 0.6$ (blue) and $H/L = 1.0$ (red). The locations of the six sections are labeled as a-f, and their locations with respect to the hill are marked in Fig. 3 with the same letters.

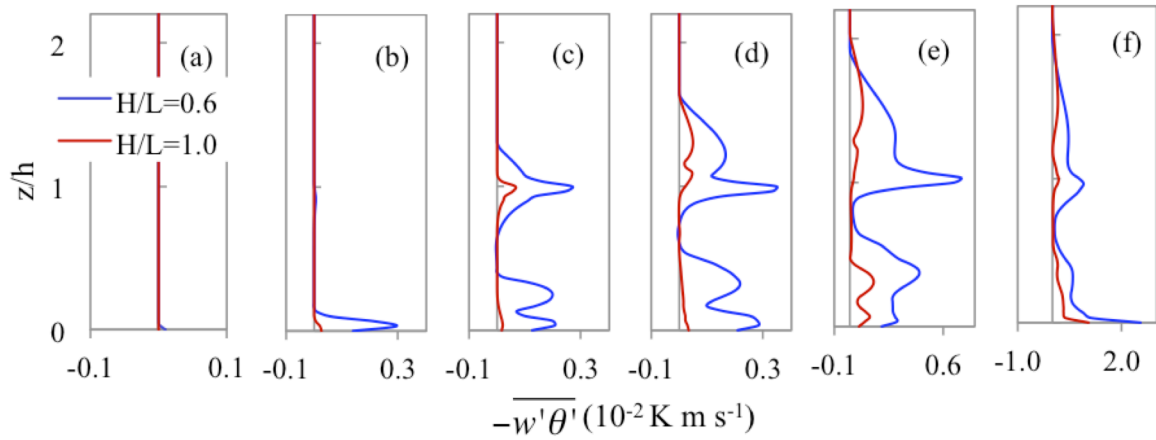


Figure 8. Profiles of turbulent Heat Flux, $-\overline{w'\theta'}$ ($10^{-2} \text{ K m s}^{-1}$) on the slope for $H/L = 0.6$ (blue) and $H/L = 1.0$ (red). The locations of the six sections are labeled as a-f, and their locations with respect to the hill are marked in Fig. 3 with the same letters.

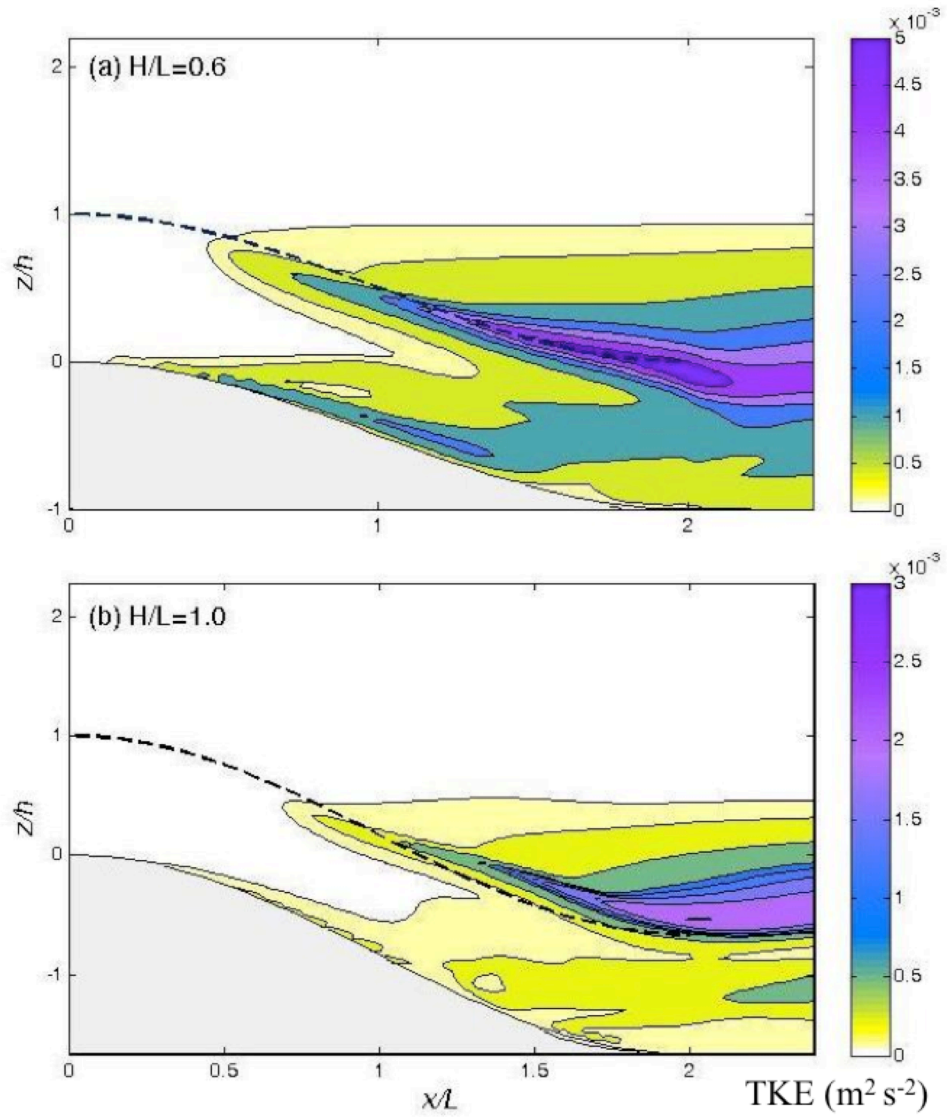


Figure 9. Contours of turbulent kinetic energy ($\text{m}^2 \text{s}^{-2}$): (a) $H/L = 0.6$; (b) $H/L = 1.0$. The black dashed lines indicate the top of canopy.

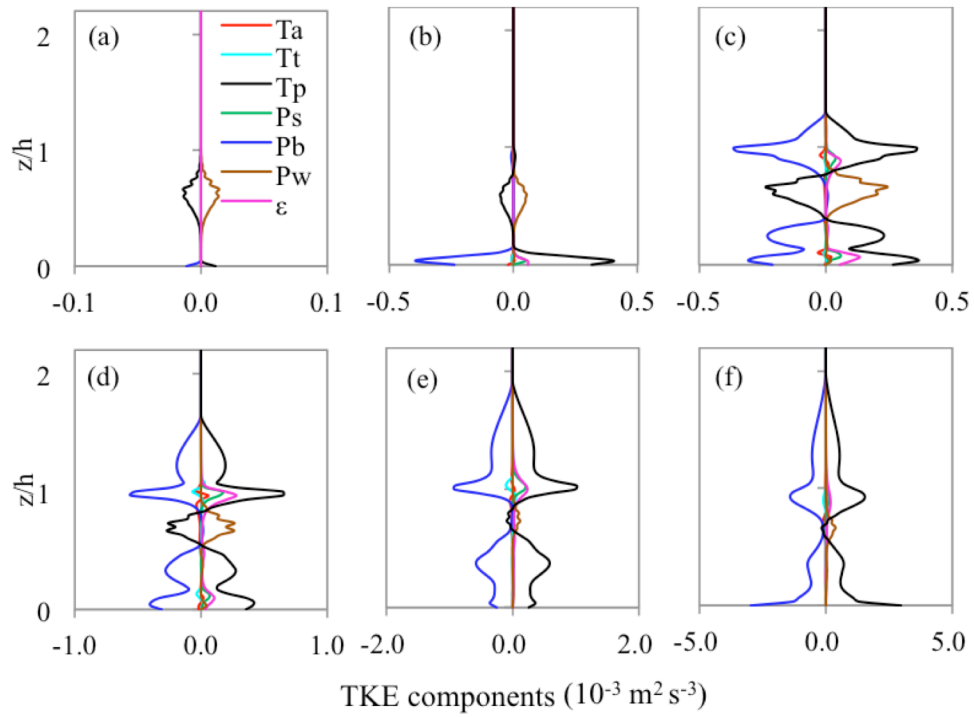


Figure 10. Profiles of TKE components ($10^{-3} \text{ m}^2 \text{ s}^{-3}$) for $H/L = 0.6$. T_a is the advection of TKE by the mean wind, T_t represents the turbulent transport of TKE, T_p represents the transport of TKE by pressure perturbation, P_s is the shear production of TKE, P_b is buoyancy production of TKE, P_w is wake production of TKE and ε is viscous dissipation of TKE. The locations of the six sections are labeled as a-f, and their locations with respect to the hill are marked in Fig. 3 with the same letters.

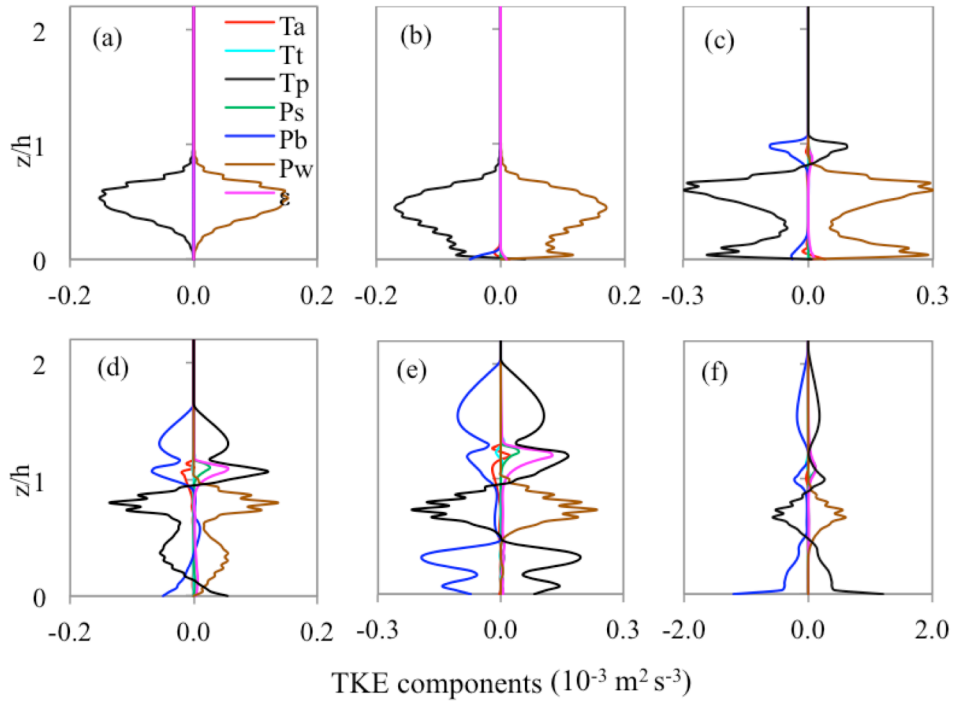


Figure 11. The same as in Fig. 10, but for $H/L = 1.0$.